Advanced Highly Reliable DC-DC Power Electronics Converters for Battery Charging Systems

By

© Jamil Muhammad Khan

A thesis submitted to the School of Graduate Studies in partial fulfillment of the requirements for the degree of Master of Engineering.

Department of Electrical and Computer Engineering

Memorial University of NewfoundLand

October, 2024

St. John's, Newfoundland and Labrador, Canada

Abstract

The thesis focuses on the development and analysis of advanced DC-DC converters, incorporating coupled inductors and interleaved PWM switching schemes to enhance efficiency and compactness. The proposed converters address key challenges in power conversion, including minimizing current ripples, reducing filter inductor size, and improving overall reliability. By leveraging high-frequency operation, these converters achieve smaller passive components and eliminate reverse recovery issues associated with MOSFET body diodes, enabling high-efficiency performance. A family of non-isolated converters was designed with features such as the doubling of effective switching frequency, common ground between input and output terminals, and the elimination of short-circuit risks. Furthermore, a novel single-phase non-isolated buck converter prototype demonstrated low current ripples and enhanced efficiency. Additionally, an isolated DC-DC buck converter was developed for renewable energy applications, incorporating phase-shift interleaving to reduce voltage stress and further optimize inductor size. The experimental results validate the proposed converters, showcasing their potential to significantly improve efficiency, reliability, and size for energy storage and electric vehicle battery charging systems.

Acknowledgements

First and foremost, I would like to express my heartfelt gratitude to my supervisor, Dr. Ashraf Ali Khan, and my co-supervisor, Dr. Mohsin Jamil, for their invaluable guidance, support, and encouragement throughout my research. Their insightful comments and immense knowledge have been crucial in the completion of this thesis.

I would also like to extend my deepest thanks to my family for their unwavering support and encouragement, which has been a constant source of strength. Additionally, I am grateful to my research colleagues particulary Frederick Nana Oppong for his collaboration and assistance, which has greatly contributed to the progress of my work.

Co-authorship Statement

I, Jamil Muahmmad khan (J.M.K), am the primary author and copyright holder of all chapters in this thesis. The simulations, methods, figures, tables and experiments were developed by me, J.M.K. The manuscripts within this thesis are co-authored by my supervisor, Dr. Ashraf Ali Khan (A.A.K), who contributed significantly to the revision and editing of the manuscripts and this thesis.

Additionally, my co-supervisor Dr. Mohsin Jamil (M.J), reviewed the experimental procedures and provided valuable suggestions for improvements. In this thesis, three publications are presented, all of which have either been completed or are currently undergoing the peer-review process. I, Jamil Muhammad Khan (J.M.K) am the primary author for all the publications. The publications are listed under the "Publications" subsection.

Table of Content

List of Figures

List of Tables

Chapter I
Introduction

1.1. Introduction

With the growing demand for clean and sustainable energy, and the increasing environmental concerns associated with fossil fuel consumption, the world is witnessing a rapid shift towards renewable energy sources (RES) [1].This transition is essential for addressing global challenges such as greenhouse gas emissions, climate change, and the depletion of natural resources. Renewable energy sources like solar, wind, and fuel cells are increasingly being integrated into energy grids and storage systems. These renewable sources are environmentally sustainable and align with the 2030 Sustainable Development Goals (SDGs). Fig.1.1 illustrates a block diagram of a renewable energy system. In this system, renewable energy sources like photovoltaics and wind power supply a stable voltage to a DC bus via DC-DC converters. The batteries serve as energy storage units, providing energy when the renewable resources are insufficient to fulfill load demand.

Similarly, Electrified transportation is essential for reducing fossil fuel reliance and minimizing environmental impacts, such as greenhouse gas (GHG) emissions and air pollution. Electric vehicles (EVs) offer a reliable, efficient, and low-maintenance zero-emission alternative to internal combustion engine (ICE) vehicles[2]. Additionally, EVs facilitate the integration of renewable energy sources (RESs) and energy storage systems (ESSs), further reducing road transport's dependence on fossil fuels and can supply back to grids in times of need[3]. A Typical EV system consist of power converters and battery storage. Power electronics, particularly DC-DC converters, play a pivotal role in enabling the efficient use and integration of RES, energy storage systems (ESS), and EVs. These converters are responsible for transforming energy between different voltage levels, ensuring that the power

generated by renewable sources or stored in batteries can be utilized effectively. [4]

Unidirectional converters allow energy flow in only one direction, typically from the power source to the load. In contrast, bidirectional converters (BDCs) enable energy transfer in both directions, making them crucial for applications involving energy storage, such as in vehicle-to-grid (V2G) systems, where energy can be both supplied to and drawn from the grid. BDCs are increasingly favored in various domains, including smart grids, hybrid EVs, and renewable energy systems, due to their versatility and efficiency.

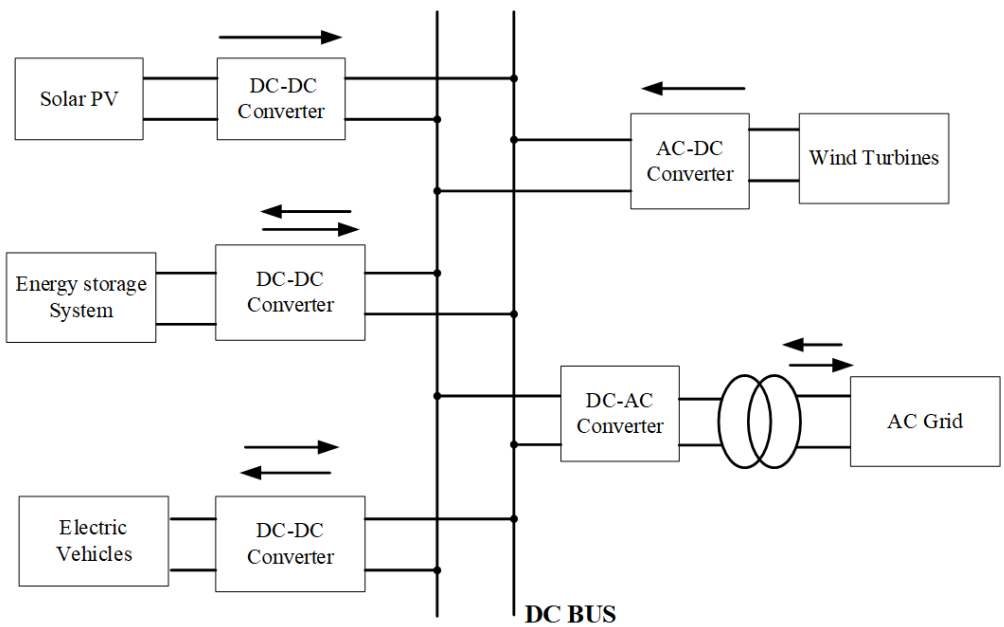

Fig.1. 1. Applicatrions of power converters in renewable energy systems.

However, conventional DC-DC converters face several challenges, such as high inductor current ripples, short-circuit risks, and increased stress on switching components, which can lead to reduced efficiency, higher power losses, and compromised reliability. Moreover, the need for dead-time in switching signals to prevent short circuits can cause distortions in output voltage waveforms, further impacting performance. Addressing these issues is crucial for

improving the efficiency and reliability of DC-DC converters, particularly in applications requiring compact, high-density power solutions.

1.2. DC-DC Converter

DC-DC converters are essential components in power electronics, enabling the conversion of direct current (DC) from one voltage level to another. These converters are widely used in applications such as renewable energy systems, electric vehicles, and battery management systems, where efficient power conversion is critical. DC-DC converters are categorized into unidirectional and bidirectional converters[5].

1.2.1. Unidirectional DC-DC Converters

These converters are designed to transfer energy in a single direction, typically from a higher voltage source to a lower voltage load, or vice versa. Common topologies include buck converters, which step down the voltage, and boost converters, which step up the voltage. Unidirectional converters are widely used in applications such as power supplies, battery charging, and renewable energy systems[6].

1.2.2. Bidirectional DC-DC Converters (BDCs)

BDCs have gained significant attention due to their ability to transfer energy in both directions. In renewable energy applications, BDCs are used to store energy in batteries when generation exceeds demand and to supply energy during periods of high demand. Similarly, in electric vehicles, BDCs manage energy flow between the battery and the motor, enabling efficient energy use during driving and regenerative braking.

Bidirectional converters (BDCs), in particular, gained significant attention in power electronics due to their widespread application in renewable energy conversion domains[5].

In [6] a bidirectional converter is derived from the unidirectional converter by replacing the diodes with switches. A bidirectional converter eliminates the need of using an extra converter for forward/reverse operations; this reduces the overall size and cost.

Based on the operating mode, the BDCs can supply power in either direction; for example, in [7] and [8] the BDCs are used to charge the battery under the condition of excess power generations. This stored energy is then used to supply power under extreme load conditions. Similarly, [2] discussed the utilization of BDCs in smart grids and plug-in hybrid electric vehicle (PHEV) charging stations. BDCs play a crucial role in the vehicle-to-grid (V2G) and grid-to-vehicle (G2V) modes. In G2V mode, the batteries are charged from the grid and in V2G mode the stored power is transferred back to the grid when needed.

1.2.3. Classification of Bidirectional Converters

BDCs are normally categorized as isolated or non-isolated converters as shown in Fig.1.2. Isolated converters have transformers in power train which provides necessary electrical isolation needed for safety purpose and common mode current reduction. In addition, the turn's ratio of the transformers can be adjusted to step-up or step-down the voltage. However, the transformer makes the circuit bulky, costly, lossy and the high turn ratios also cause high leakage inductance [9]. On the other hand the non-isolated converters lack the advantage of galvanic isolation. However, the non-isolated converters are preferred to achieve higher efficiency and reduce size, weight, and cost. For example, the non-isolated type is the more favorable choice in high-power applications and applications relating to spacecraft power systems, where minimizing weight and size are primary considerations. For common mode leakage reduction and safety purpose the non-isolated converters need to have a common ground[10].where isolation is not required.

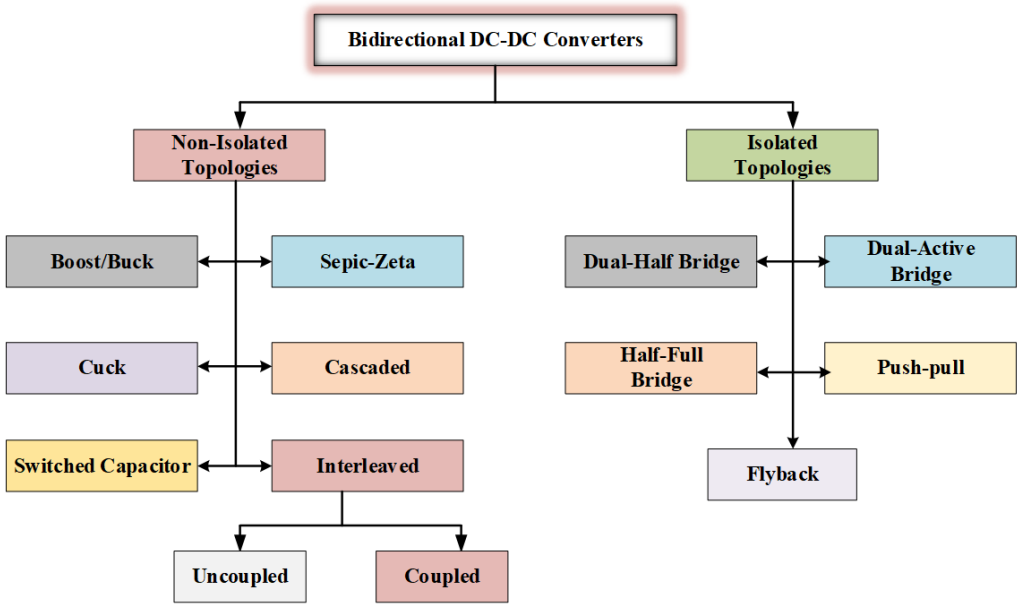

Fig.1. 2. Classification of Bidirectional DC-DC Converter

1.2.3. Challenges and development in Bidirectional DC-DC converters

The design and development of DC-DC converters have been explored in the literature, with a focus on improving efficiency, reliability, and power density. Recent research has concentrated on bidirectional converters due to their applicability in energy storage systems, renewable energy integration, and electric vehicles.

Conventional BDCs, such as buck, boost, and buck-boost converters, are well-known for their simplicity and cost-effectiveness. However, these converters face challenges related to high current ripples [11], [12], which can lead to electromagnetic interference (EMI), increased power losses, and reduced battery life. Additionally, conventional BDCs require dead-time in switching signals to prevent short circuits, which can cause output voltage distortions and reduce overall efficiency.

Current ripple can be decreased by increasing the inductance of the inductors. However, the large inductor size slows down the dynamic response of the converter [13]. Interleaving technique is used to reduce the inductor ripple. The inductor current ripple can be decreased by introducing a phase shift between the switching instant of the interleaved channels. However, the number of switches and inductors are increased, which increases the control complexity and cost of the converter. Furthermore, Cascaded converter with phase shifts can be used to decrease the inductor ripples, but it can increase the number of switches and inductors[14].

The use of coupled inductors in DC-DC converters has also been investigated to enhance efficiency and reduce component size. Coupled inductors can improve the voltage conversion ratio and reduce switching losses, making them suitable for high-frequency applications. However, the challenge of leakage inductance and voltage spikes on switches remains a concern, often requiring additional snubber circuits to mitigate these issues

1.3. Problem Statement and Motivations

The increasing adoption of renewable energy sources and electric vehicles has underscored the need for advanced DC-DC converters that can provide high efficiency, low ripple, and minimal component stress while maintaining compactness and reliability. Conventional bidirectional DC-DC converters, despite their widespread use, often suffer from several limitations, including high current ripples, short-circuit risks, and significant stress on switching components. These challenges not only reduce the efficiency and lifespan of the converters but also make them less suitable for applications requiring high power density and reliability. Furthermore, the health and efficiency of energy storage system is dependent on the output of the charging current. Ripples in charging current can cause heating and reduce the lifetime of batteries.

To address these challenges, there is a need to develop innovative DC-DC converter designs that eliminate short-circuit risks, reduce current ripples, and operate at high switching frequencies without the drawbacks associated with traditional designs.

1.4. Research Objectives

This research aims to propose novel bidirectional and unidirectional DC-DC converter topologies that incorporate coupled inductors, interleaving techniques, and advanced control strategies to enhance performance. These converters aim to achieve high efficiency, low voltage and current stress, reduced component count, and improved power density, making them ideal for applications in energy storage systems, renewable energy integration, and electric vehicle battery management.

This thesis aims to design and analyze novel bidirectional DC-DC converters family topology focusing on buck and boost converters, and a novel unidirectional DC-DC Buck Converter for low voltage on board charging converters, to address voltage sag/swell, foundations, voltage gain and quality. The specific objectives of this research are as follows:

- Design and analyze advanced DC-DC Converters for battery charging applications.
- Mathematical modeling, analysis, loss analysis and simulation of proposed converters.
- Hardware prototype and analysis and verifications of results.

1.5. Thesis Overview

This thesis is structured into four main chapters, each addressing a specific aspect of DC-DC converter design and analysis:

- **Chapter 1:** This chapter introduces the research by highlighting the importance of

power conversion systems for renewable energy storage systems and electric vehicles (EVs). It discusses the development and challenges in DC-DC converters, identify the problem statement for the need for efficient converters and explains research objectives.

- **Chapter 2:** This chapter introduces a novel family of bidirectional DC-DC converters focused on boost conversion. The proposed converters feature no short-circuit issues, no dead time in switching signals, and no reverse recovery problems in MOSFETs, making them highly efficient and suitable for high-frequency operation. The chapter concludes with the advantages of the proposed converters in terms of component stress reduction and common ground maintenance.
- **Chapter 3:** This chapter presents a non-isolated bidirectional DC-DC Buck converter designed for battery charging, focusing on buck conversion. The proposed converter minimizes output ripple, reduces inductor size, and eliminates the need for additional snubber circuits, making it an effective solution for low-voltage on-board charging applications.
- **Chapter 4:** This chapter discusses a unidirectional isolated DC-DC buck converter suitable for battery charging applications. The proposed design operates the output inductor at four times the switching frequency, allowing for a much smaller inductor and reduced diode stress. The chapter demonstrates how this design enhances efficiency and reliability in EV and renewable energy system (RES) applications.
- **Chapter 5:** The final chapter summarizes the key findings of the research, highlights the contributions made to the field of DC-DC converter design, and suggests directions for future research.

References

[1] O. Edenhofer, R. Pichs Madruga, Y. Sokona, and IPCC, Eds., *Renewable energy sources and climate change mitigation: summary for policymakers and technical summary*. Genf: International Panel of Climate Change, 2011.

[2] Y. Du, X. Zhou, S. Bai, S. Lukic, and A. Huang, "Review of non-isolated bi-directional DC-DC converters for plug-in hybrid electric vehicle charge station application at municipal parking decks," in *2010 Twenty-Fifth Annual IEEE Applied Power Electronics Conference and Exposition (APEC)*, Palm Springs, CA, USA: IEEE, Feb. 2010, pp. 1145–1151. doi: 10.1109/APEC.2010.5433359.

[3] N. Sujitha and S. Krithiga, "RES based EV battery charging system: A review," *Renew. Sustain. Energy Rev.*, vol. 75, pp. 978–988, Aug. 2017, doi: 10.1016/j.rser.2016.11.078.

[4] S.-P. Wang, H. Liao, and J.-F. Chen, "Design and Implementation of a Novel Bidirectional DC-DC Converter with Coupled Inductor," in *2018 IEEE 7th World Conference on Photovoltaic Energy Conversion (WCPEC) (A Joint Conference of 45th IEEE PVSC, 28th PVSEC & 34th EU PVSEC)*, Waikoloa Village, HI: IEEE, Jun. 2018, pp. 0644–0649. doi: 10.1109/PVSC.2018.8548196.

[5] A. P. Kumar, V. V. S. K. Bhajana, and P. Drabek, "A novel ZCS interleaved bidirectional buck-boost DC-DC converter for energy storage applications," in *2016 ELEKTRO*, Strbske Pleso, High Tatras, Slovakia: IEEE, May 2016, pp. 180–185. doi: 10.1109/ELEKTRO.2016.7512061.

[6] A. A. Khan, Honnyong Cha, and H. F. Ahmed, "A family of high efficiency bidirectional DC-DC converters using switching cell structure," in *2016 IEEE 8th International Power Electronics and Motion Control Conference (IPEMC-ECCE Asia)*, Hefei, China: IEEE, May 2016, pp. 1177–1183. doi: 10.1109/IPEMC.2016.7512455.

[7] K. Tytelmaier, O. Husev, O. Veligorskyi, and R. Yershov, "A review of non-isolated

bidirectional dc-dc converters for energy storage systems," in *2016 II International Young Scientists Forum on Applied Physics and Engineering (YSF)*, Kharkiv, Ukraine: IEEE, Oct. 2016, pp. 22–28. doi: 10.1109/YSF.2016.7753752.

[8] "IET Power Electronics - 2014 - Chao - Bidirectional DC DC soft-switching converter for stand-alone photovoltaic power (1).pdf."

[9] Netaji Subhas and A. Singh, "High Voltage Gain Bidirectional DC-DC Converters for Supercapacitor Assisted Electric Vehicles: A Review," *CPSS Trans. Power Electron. Appl.*, vol. 7, no. 4, pp. 386–398, Dec. 2022, doi: 10.24295/CPSSTPEA.2022.00035.

[10] P. H. Feretti, F. L. Tofoli, and E. R. Ribeiro, "Family of Non-Isolated High Step-Up DC–DC Converters Based on the Multi-State Switching Cell," *IEEE J. Emerg. Sel. Top. Power Electron.*, vol. 10, no. 5, pp. 5882–5893, Oct. 2022, doi: 10.1109/JESTPE.2022.3160280.

[11] G.-R. Zhu, S.-C. Tan, Y. Chen, and C. K. Tse, "Mitigation of Low-Frequency Current Ripple in Fuel-Cell Inverter Systems Through Waveform Control," *IEEE Trans. Power Electron.*, vol. 28, no. 2, pp. 779–792, Feb. 2013, doi: 10.1109/TPEL.2012.2205407.

[12] A. Abrishamifar, S. Samadi, and A. Ale Ahmad, "Low-frequency current ripple reduction in front-end boost converter with single-phase inverter load," *IET Power Electron.*, vol. 5, no. 9, pp. 1676–1683, Nov. 2012, doi: 10.1049/iet-pel.2011.0470.

[13] Po-Wa Lee, Yim-Shu Lee, D. K. W. Cheng, and Xiu-Cheng Liu, "Steady-state analysis of an interleaved boost converter with coupled inductors," *IEEE Trans. Ind. Electron.*, vol. 47, no. 4, pp. 787–795, Aug. 2000, doi: 10.1109/41.857959.

[14] W. C. Leal, M. O. Godinho, R. F. Bastos, C. R. De Aguiar, G. H. F. Fuzato, and R. Q. Machado, "Cascaded Interleaved DC–DC Converter for a Bidirectional Electric Vehicle Charging Station," *IEEE Trans. Ind. Electron.*, vol. 71, no. 4, pp. 3708–3717, Apr. 2024, doi: 10.1109/TIE.2023.3273281.

Chapter II
A Family of Couple inductor based Bidirectional Converter (Boost Converter)

Preface

A section from this chapter has been submitted and accepted in NECEC 2023. I, Jamil M Khan (J.M.K) the primary author of this manuscript. Conceptualization, J.M.K, and my supervisor Ashraf Ali Khan (A.A.K), Investigation, A.A.K; Methodology J.M.K, Funding Acquisition, A.A.K; Supervision: A.A.K; Writing-Review and Editing J.M.K. All authors have read and agreed to the published version of the manuscript.

Abstract

This article presents a family of non-isolated bidirectional dc-dc converters using coupled inductors and interleaved PWM scheme. The effective switching frequency of the filter inductors is twice of the actual switching frequency and the filter inductors have less voltages; as a result the input/output current ripples can be much smaller. In addition, the size of the filter inductors can be much decreased which makes the converter efficient. The body didoes of switches do not show any reverse recovery issues which enabled the utilization of MOSFETs along with fast external diodes for high-switching and high-efficiency operation. The proposed converters can be operated at high frequency to reduce the size of passive components. Moreover, the proposed converters have no short-circuit issues which leads to a high reliability. Furthermore, the proposed converters do not require dead time which leads to a better output voltage gain and good quality waveforms with less distortion. The proposed converters preserve a common ground between the input and output terminals, this eliminates the issue of common mode current. In this article the boost type converter is analyzed in detail and the same analysis can be extended into the other converters.

2.1. Introduction

With the increase in energy demands and growing concern for the global environment, there has been rapid growth in obtaining clean and sustainable energy using renewable energy sources (RES). Improvements in power converters have further contributed to this growth [1], [2]. Bidirectional converters (BDCs), in particular, gained significant attention in power electronics due to their widespread application in renewable energy conversion domains[3]. Unlike conventional unidirectional converters, bidirectional converters allow current flow in both directions, that is, from source to load and vice versa [4]. In [5] a bidirectional converter is derived from the unidirectional converter by replacing the diodes with switches. A bidirectional converter eliminates the need of using an extra converter for forward/reverse operations; this reduces the overall size and cost. The general configuration of a bidirectional converter is shown in Fig. 2.1.[5], where V_1 is input voltage, V_2 is output voltage, I_1 is input current and I_2 is input current. The application of these converters are but not limited to smart grids [6], [7], hybrid electric vehicles (EVs) [8], uninterrupted power supplies (UPS) [9], space craft's [10], and renewable energy systems [11] such as photovoltaic (PVs) [12], wind turbines [13], and fuel cells [14].

Based on the operating mode, the BDCs can supply power in either direction; for example, in [15] and [16] the BDCs are used to charge the battery under the condition of excess power generations. This stored energy is then used to supply power under extreme load conditions . Similarly, [17] discussed the utilization of BDCs in smart grids and plug-in hybrid electric vehicle (PHEV) charging stations. BDCs play a crucial role in the vehicle-to-grid (V2G) and grid-to-vehicle (G2V) modes. In G2V mode, the batteries are charged from the grid and in V2G mode the stored power is transferred back to the grid when needed.

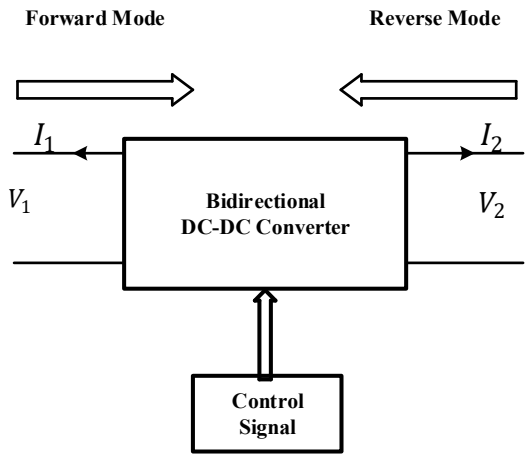

Fig.2. 1. General configuration of a dc-dc bidirectional converter.

BDCs are normally categorized as isolated or non-isolated converters. Isolated converters have transformers in power train which provides necessary electrical isolation needed for safety purpose and common mode current reduction. In addition, the turn's ratio of the transformers can be adjusted to step-up or step-down the voltage. However, the transformer makes the circuit bulky, costly, lossy and the high turn ratios also cause high leakage inductance [18]. On the other hand the non-isolated converters lack the advantage of galvanic isolation. However, the non-isolated converters are preferred to achieve higher efficiency and reduce size, weight, and cost. For example, the non-isolated type is the more favorable choice in high-power applications and applications relating to spacecraft power systems, where minimizing weight and size are primary considerations. For common mode leakage reduction and safety purpose the non-isolated converters need to have a common ground[19].

Conventional BDCs such as simple buck, boost, inverting buck-boost and non-inverting buck-boost converters are the famous non-isolated converters. However, they suffer from several drawbacks as discussed below. The switches of BDCs in the same leg operates at complementary PWM strategy, when one switch is ON the other is OFF but both cannot be ON at the same time. Therefore, conventional BDCs have short circuit risk and requires finite

dead-time in the switching signals. But inserting dead-time causes distortions in the output voltage waveforms and leading to a reduced voltage gain. This issue becomes more severe as the converter switching frequency increases.

Furthermore, in hard switching converters, the switching loss increases, and the reverse recovery of the body diode becomes more severe. MOSFETs can effectively decrease switching and conduction losses due to their faster switching capability, lack of turn-off tail current, and absence of fixed voltage drops [20]–[22]. However, MOSFETs are not designed with high reverse recovery features and can suffer device failure, which can further lead to EMI problems. On the other hand IGBTs can be used to solve device failure issue due to its relatively fast body diodes, but it has low switching speed and fixed voltage drop [23], [24].

Moreover, the conventional BDCs have higher inductor current ripples. The effects of current ripples on energy storage devices are discussed in [25], [26]. The current ripple causes EMI noise, and internal heating which leads to poor battery life and higher power losses. Current ripples can be minimized using the following techniques.

1. Current ripple can be decreased by increasing the inductance of the inductors. However, the large inductor size slows down the dynamic response of the converter [27].
2. Increasing the switching frequency can reduce the ripple current and inductor size. However, the switching frequency is limited by the gate drive circuit, switching losses, and electromagnetic compliance requirements.
3. The discontinuous conduction mode (DCM) in converters can reduce the inductance of the input inductors. However, the large input inductor current in the DCM mode increases the switch current, leading to increased power loss, higher EMI noise, and increases filtering requirements.
4. Interleaving technique is used to reduce the inductor ripple. The inductor current ripple can be decreased by introducing a phase shift between the switching instant of the interleaved

channels. However, the number of switches and inductors are increased, which increases the control complexity and cost of the converter.

5. Cascaded converter with phase shifts can be used to decrease the inductor ripples, but it can increase the number of switches and inductors.

In order to improve the dynamic response of the non-isolated BDCs, coupled inductors are utilized in [32] and [33]. The switching frequencies of the converters are rapidly increasing with the development of wideband gap devices. Therefore, the need for converters that can operate at high frequencies and exhibit high power density and efficiency has increased.

This paper presents a family of non-isolated coupled inductor-based BDCs as shown in Fig. 2.2. The proposed topologies use interleaved switching scheme and have mitigated the issues associated with conventional BDCs. The proposed BDCs have the following main benefits.

1. No short-circuit issues.
2. No dead-time is required in the switching signals.
3. The body diodes of the switching device do not conduct in the given configuration. Therefore, MOSFETs do not show any reverse recovery issues and can be operated at higher switching frequencies.
4. The effective switching frequency of the filter inductors is twice of the actual switching frequency, this minimizes the size of the filter inductors, which could increase the dynamic response.
5. The proposed converters preserves a common ground between the input and output terminal, eliminating the common-mode current.
6. Due to no reverse recovery issues and absence of dead time in the switching signals the converter can be operated at high switching frequency and high efficiency can be realized.

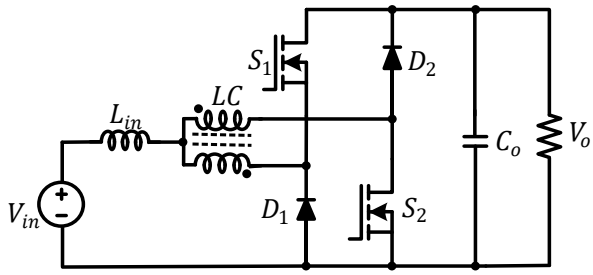

(a)

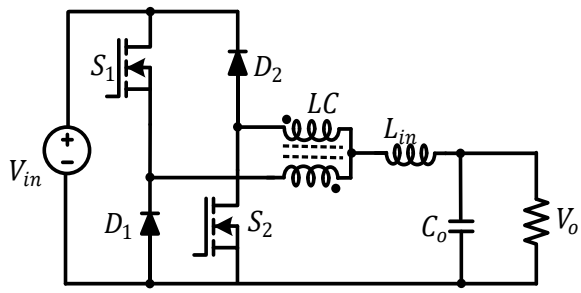

(b)

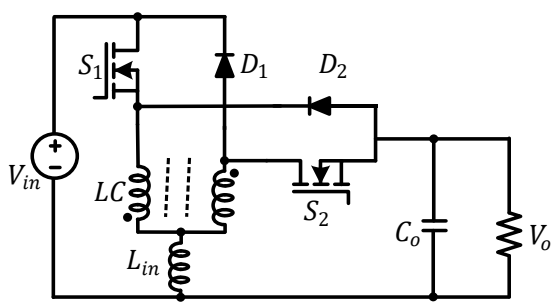

(c)

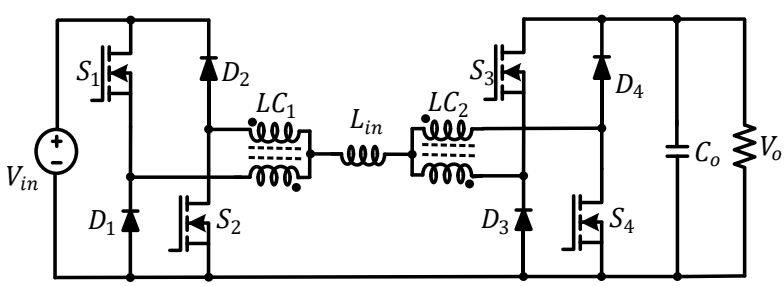

(d)

Fig. 2.2 Family of the proposed converters without magnetic integration. (a) Boost converter. (b) Buck converter. (c) Inverting buck-boost converter. (d) Non-inverting buck-boost converter.

2.2. Proposed Circuit Topology

A family of the proposed BDCs is shown in Fig. 2.2. Figs. 2.2(a), (b), (c) and (d) show the proposed boost, buck, inverting buck-boost and non-inverting buck-boost converters, respectively. The proposed buck converter generates output dc voltage lower or equal to input dc voltage. The proposed boost converter generates output dc voltage higher or equal to input dc voltage. The proposed inverting buck-boost converter generates output dc voltage higher or equal to input dc voltage but opposite in polarity to the input voltage. The proposed non-inverting buck-boost converter generates output dc voltage higher or equal to input dc voltage and in the same polarity as the input voltage. As shown in the switching legs of the converters have one MOSFET and one external diode connected in series which eliminates the risk of short-circuit. For example, the proposed boost converter in Fig. 2.2(a) has two power MOSFETs (S_1, S_2), two freewheeling diodes (D_1, D_2), one coupled inductor (LC), one input filter inductor (L_{in}) and an output capacitor (C_o). The freewheeling diodes can be chosen externally with fast recovery features and low turn-on resistance. The coupled inductor is used to limit short-circuit, stop the flow of current through the body diodes of MOSFETs and increase effective switching frequency of the input inductor by twice.

2.3. Modulation Strategy of the Proposed Converter

The proposed converter utilizes inverted-interleaved PWM switching scheme as shown in Fig. 2.3. The PWM switching scheme is created by comparing two triangular waves, v_{tr1} and v_{tr2}, which are 180 degrees out of phase, with a reference voltage v_{ref}. It is important to highlight that S_2 is the complement of signal produced by v_{tr2} and v_{ref}. It has both dead time and overlap time operation mode.

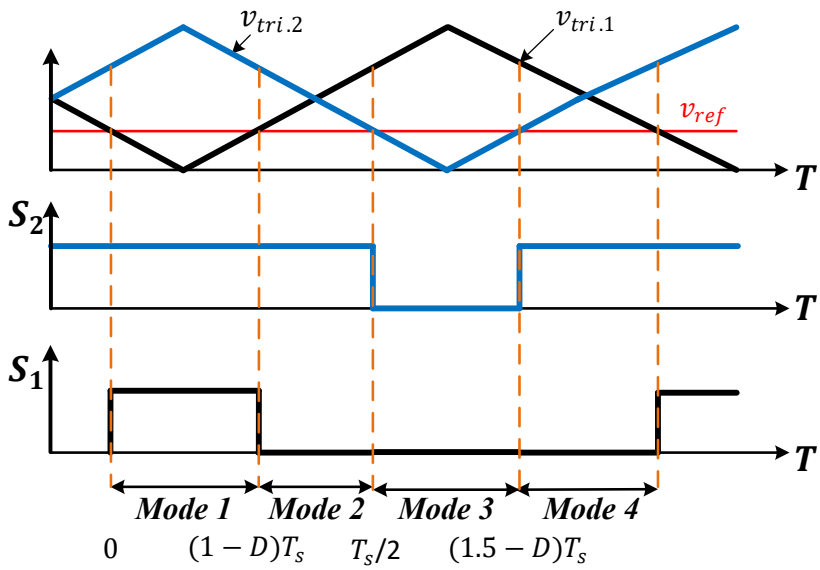

Fig. 2.3. Interleaved switching scheme of the proposed converter.

2.4. Operation Principle of the Proposed Converter

The boost converter shown in Fig. 2.2(a) is selected and analyzed in this paper and similar analysis can be extended to the other converters. The proposed topologies have four continuous conduction modes as shown in Fig. 2.4.

In Fig. 2.4(a). , there are two distinct current components: the input inductor current (I_{lin}) and the common mode current (I_{cm}), also known as circulating current. The common mode current is calculated as the average of the winding currents (I_{L1} and I_{L2}), while the input inductor current is determined as the difference between the winding currents. From Fig. 2.5. the equation for common mode current and Input inductor current is given by

$$\begin{cases} I_{cm} = \dfrac{I_{L_1} + I_{L_2}}{2} \\ I_{Lin} = I_{L_1} - I_{L_2} \end{cases} \tag{2.1}$$

In this section the couple inductor is assumed with unity coupling and zero leakage inductance. As shown in Fig. 4, the duty cycle D is defined as the time interval when S_1 is on

during one switching period T_s.

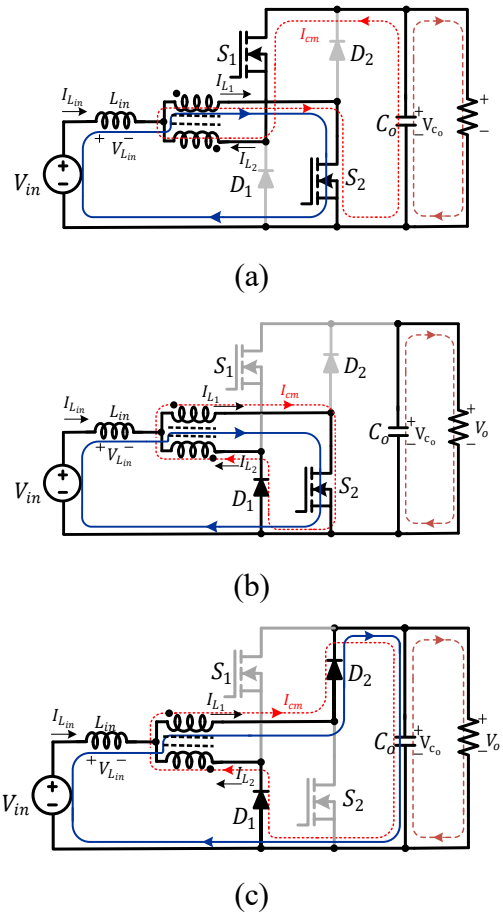

Fig. 2.4. Operation modes of the proposed converter. (a) Mode 1. (b) Mode 2. (c) Mode 3.

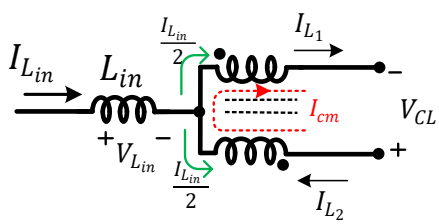

Fig.2.5. Common mode and input inductor current.

Mode 1 [0 - $(1-D)T_s$]

As depicted in Fig. 2.4(a), in this operating mode, both switches S_1 and S_2 are active, and the diodes D_1, and D_2 are in a reverse-biased condition. In this mode, Input Inductor L_{in} stores energy, and the output voltage is provided by capacitor C_o. By applying KVL across the input current path, voltage across input inductor is given by

$$V_{L_{in}} = V_{in} - V_{L_1} \tag{2.2}$$

Similarly, applying KVL across the common mode current path, we obtain

$$V_{L_1} = V_{C_o} - V_{L_2} \tag{2.3}$$

Since, for tight coupling,

$$\begin{cases} V_{L_1} = V_{L_2} \\ V_{C_o} = V_o \end{cases} \tag{2.4}$$

Substituting (2.4) into (2.1), (2.2) and (2.3) results in

$$\begin{cases} V_{L_1} = V_o - V_{L_1} \\ V_{L_1} = \dfrac{V_o}{2} \\ V_{L_{in}} = V_{in} - \dfrac{V_o}{2} \end{cases} \tag{2.5}$$

$$V_{L_{in}} = L_{In}\frac{dI_{L_{in}}}{dt} \tag{2.6}$$

Mode 2 [$(1-D)T_s$) - $T_s/2$)]

Mode 2 is shown in Fig. 2.4(b). The switch S_1 is turned OFF, and S_2 is ON, the diode D_1 is conducting only the circulating current due to freewheeling action, and D_2 remain OFF.

$$\begin{cases} V_{in} = V_{L_{in}} + V_{L_1} \\ V_{in} = V_{L_{in}} - V_{L_1} \end{cases} \tag{2.7}$$

From the above equation we get

$$V_{L_{in}} = V_{in} \tag{2.8}$$

Mode 3 [$T_s/2$-$(1.5 - D)T_s$]

Mode 3 is shown in Fig. 2.4(c). Both the switches S1 and S2 are inactive and both diodes D_1 and D_2 are conducting.

Mode 4 [$(1.5 - D)T_s$- T_s]

Mode 4 is the same as Mode 2 as shown in Fig.2.4(b).

The gain equation for the proposed converter is obtained by using equations (2.5) and (2.7) and applying Volt-Sec balance condition on the input inductor (L_{In}) as below.

$$\frac{V_o}{V_{in}} = \frac{1}{1 - D} \tag{2.9}$$

2.5. Design Specifications and ripple analysis

2.5.1. Input Inductor Ripples

The Current ripple ΔI_{in} of the input inductor L_{In} can be calculated from (2.5) and (2.6)

$$L_{In} \frac{dI_{L_{in}}}{dt} = V_{in} - \frac{V_o}{2} \tag{2.10}$$

By putting the values of V_{in} from (2.9), equation (2.12) become

$$\begin{cases} L_{In} \frac{dI_{L_{in}}}{dt} = V_o(1 - D) - \frac{V_o}{2} \\ \Delta I_{L_{in}} = \frac{2V_o(1-D)-V_o}{2L_{In}} D.T_s \\ \Delta I_{L_{in}} = \frac{V_o(D-2D^2)T_s}{2L_{In}} \end{cases} \tag{2.11}$$

From (2.11), maximum ripples in the inductor current occur at D = 0.25 where $V_o = V_{o(\max)}$ and $T_s = \frac{1}{f_s}$ is the switching period of the converter. Equation (2.11), in terms of input voltage, can be written as

$$\Delta I_{in} = \frac{V_{in}(D - 2D^2)T_s}{2(1 - D)L_{In}} \tag{2.12}$$

2.5.2. Input Inductor Design

From equation (2.9) and (2.10), the input inductor equation can be derived as

$$L_{In}\frac{dI_{L_{in}}}{dt} = \frac{(V_{in} - 2V_{in}D)}{2(1-\mathrm{D})} \tag{2.13}$$

From equation (2.12)

$$\begin{cases} L_{In} \geq \dfrac{(V_{in} - 2V_{in}D)DT_s}{2(1 - \mathrm{D})\ \Delta I} \\ L_{in} \geq \dfrac{V_{in}(D - 2D^2)}{\Delta \mathrm{I} f_{sw}} \end{cases} \tag{2.14}$$

$\Delta \mathrm{I} = \mathrm{x}\% I_{in}$, with x% denoting the maximum allowable current ripple for the inductors.

$$L_{in} \geq \frac{{V_{in}}^2 D(1 - 2D)}{2(1 - \mathrm{D})\mathrm{x}\% I_{in} f_s} \tag{2.15}$$

Assume that the converter is lossless, i.e. $P_{out} = P_{in}$. Equation (2.14) can be written as

$$L_{in} \geq \frac{{V_{in}}^2 D(1-2D)}{2(1-\mathrm{D})\mathrm{x}\% P_{out} f_s} \tag{2.16}$$

2.5.3. Coupled Inductor Design

Equation for the common mode current is obtained by applying KVL along the current path as given below

$$L\frac{dI_{cm}}{dt} = V_{co} \tag{2.17}$$

Where L is the inductance of coupled inductor, common mode current can be written in terms of mutual inductance(L_M) as below

$$\begin{cases} \dfrac{dI_{cm}}{dt} = \dfrac{V_{co}}{4L_M} \\ \Delta I_{cm} = \dfrac{V_{c_0} DT_s}{4L_M} \end{cases} \tag{2.18}$$

In the above equation ΔI_{cm} is the common mode ripple current.

From Fig.6. The winding current of the coupled inductor can be expressed in terms of i_{cm} and $i_{L_{in}}$ as below.

$$I_{L1} = I_{cm} + \frac{I_{L_{in}}}{2} \tag{2.19}$$

$$I_{L2} = I_{cm} - \frac{I_{L_{in}}}{2} \tag{2.20}$$

The equation for the coupled inductor current ripple can be obtained by putting values from equations (2.11) and (2.18) into (2.19) as follows

$$\begin{cases} I_{L1} = \dfrac{V_{co}}{4L_M} + \dfrac{V_o(D - 2D^2)T_s}{4L_{in}} \\ I_{L1} = \left(\dfrac{1}{L_M} + \dfrac{1}{L_{in}} - \dfrac{2D}{L_{in}}\right) V_o D T_s \end{cases} \tag{2.21}$$

The maximum ripples occurs when $\frac{2D}{L_{in}} \approx 0$. Using large values of L_M can also reduce the ripple current of the couple inductor, but the presence of an air gap in the couple inductor for switching cell structure reduces the size of L_M.

In comparison to the conventional DC-DC converter, the input inductor (L_{in}) of proposed converter encounters twice of the switching frequency, this enables us to choose a very small value of the input inductor (L_{in}) as compared to the conventional converter. Furthermore, the current ripple is shared between the two inductors (L_1 and L_2) which reduces the overall current ripple, especially at higher conversion ratios. Similarly due to the division of current the voltage and current stress across the switches are low.

2.5.4. Inductance comparison of the conventional and proposed converter

The equation for the current ripples of the proposed converter is given in equation

(2.11). For conventional converter the equation is given as

$$\Delta I_{in\_conv} = \frac{V_o(1-D)DT_s}{L_{In.conv}} \tag{2.22}$$

By comparing (2.11) and (2.22), the ration of conventional versus propose input induction ($L_{In.conv}/L_{In}$) can be written as.

$$L_{in_{conv}}/L_{in} = \frac{(1-D)}{(0.5-D)} \tag{2.23}$$

Fig.2.6. illustrates the necessary inductance value for the conventional DC-DC converter in order to sustain an equivalent input inductor current ripple as observed in the proposed converter, with variations in duty ration *(D)* from 0 to 0.5. As depicted, the input inductance for the conventional DC-DC converters ($L_{In.conv}$) is notably larger compared to that of the proposed converter ($L_{in_{conv}}$). For example, when D = 0.47, $L_{In.conv}$ is nearly 17.6 times the size of proposed input inductor L_{in}.

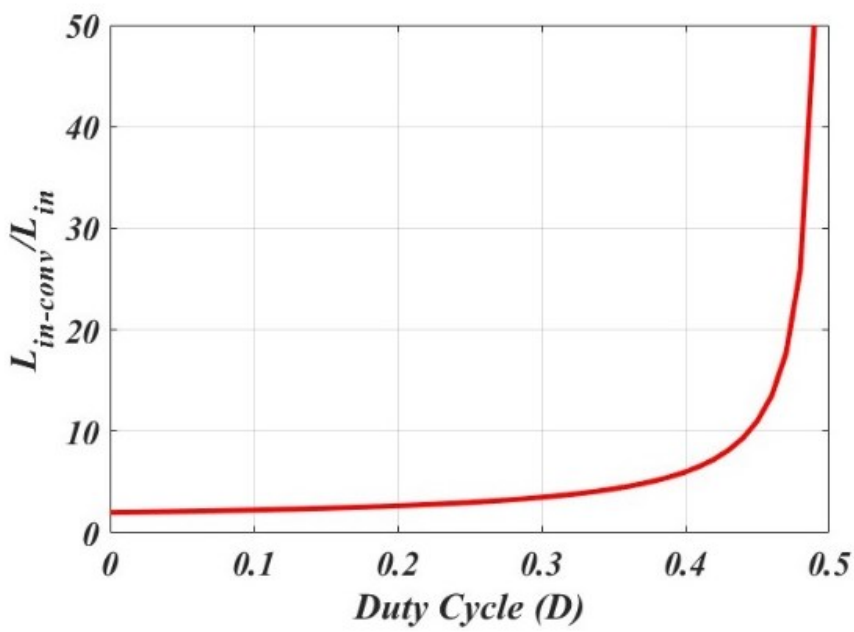

Fig. 2.6. Input inductor ratio for the conventional vs proposed converter.

2.6. Simulation Results of the Proposed DC-DC Converter

The proposed boost converter configuration was modeled using MATLAB to deliver 200 watts of power. The following parameters were used. A 48-volt input DC voltage (V_{in}), Input inductance (L_{in}) of 0.1mH, coupled inductor (LC) with coupling factor $k=1$, and output capacitor (C_o) of 1uF. The design equations derived in earlier sections were applied to determine the specific component values as shown in Table 2.1. The operating frequency (f_s) of the converter is 50 kHz. In order to achieve the desired output voltage (V_o) of 205 volts, the converter was operated with a duty ratio (D) of 0.76. The key waveforms are shown in Fig. 2.7,Fig.2.8 and Fig.2.9. Fig. 2.7(a) illustrate the input voltage (V_{in}) and output voltage (V_o) waveforms

Table 2.1

Components Specifications (Bidirictional Boost Converter)

Components	***Values***
Input voltage (V_{in})	48 V
Output voltage (V_{out})	205 V
Rated output power	400 W
MOSFET (S_1)	NTHL065N65S3HF
Switching frequency	50Khz
Diodes ($D_1 - D_2$)	BYC30JT-600PSQ
Inductors (L_{in})	0.176 mH
Output Capacitor (C_O)	100 μF

Fig. 2.7(b) illustrates the current waveforms of the coupled inductor L_1 and L_2. Fig. 2.7(c) displays the common mode current (I_{cm}) and Fig. 2.7(d) shows the output current waveform of the proposed converter. Fig. 2.8. Illustrates Input Inductor current

(I_{L1}) against Switches S_1 and S_1 showing I_{L1} has twice frequency as compared to switching frequency.

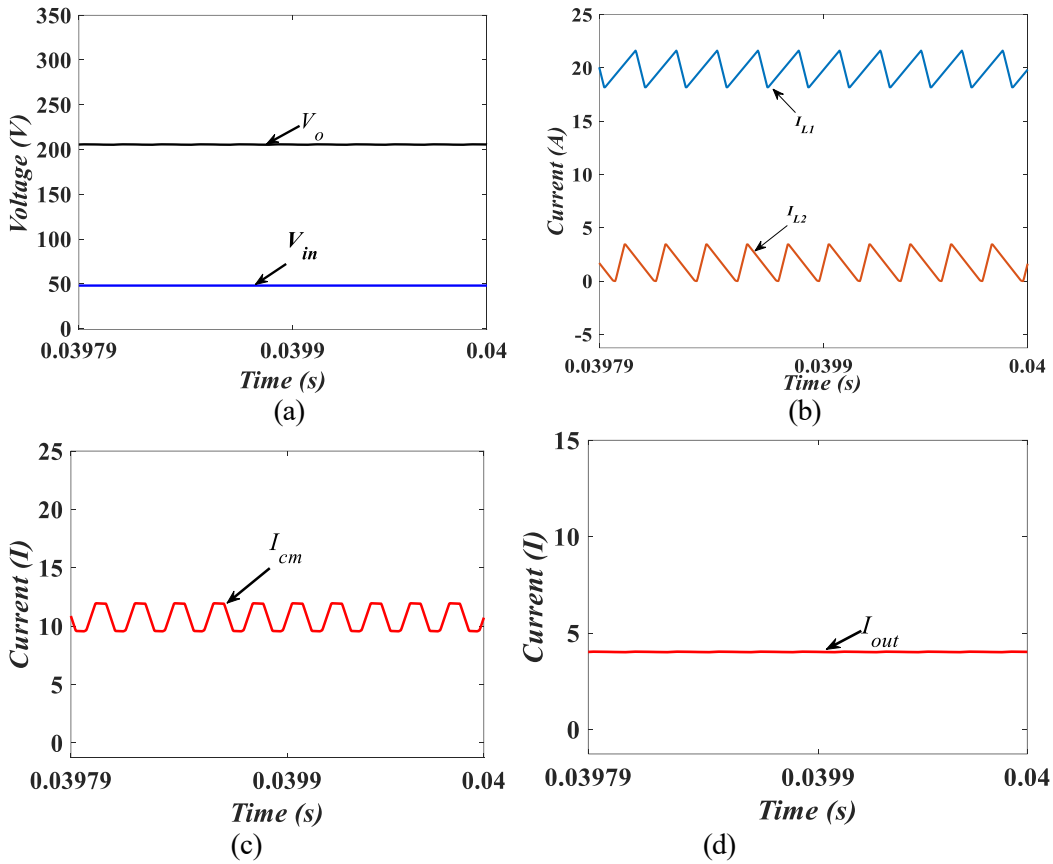

Fig. 2.7. Simulation results. (a) Input and output voltages. (b) Inductors L_1 and L_2 current waveforms. (d) Inductor I_{Cm} voltage waveform. (e) Output current waveform I_o.

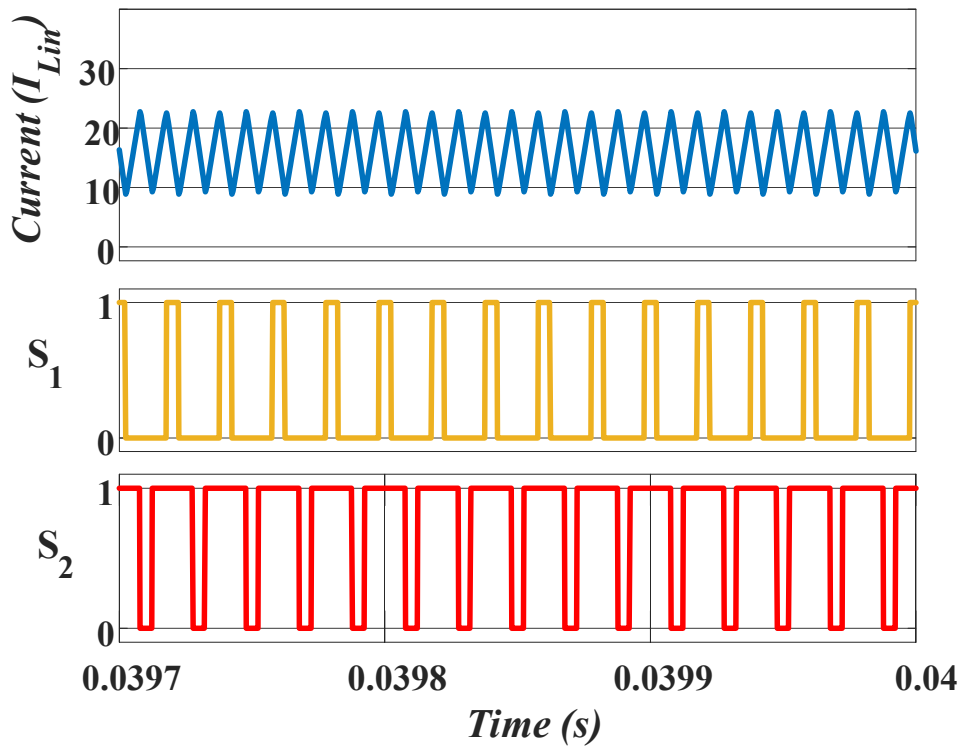

Fig. 2.8. Input Inductor current (I_{L1}) against Switch (S_2) and Switch (S_1) showing I_{L1} has twice frequency as compared to Switching Frequency.

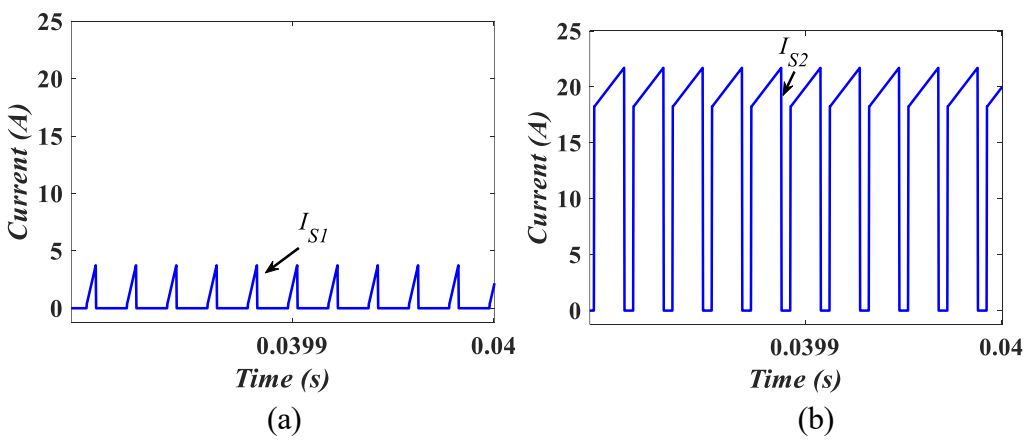

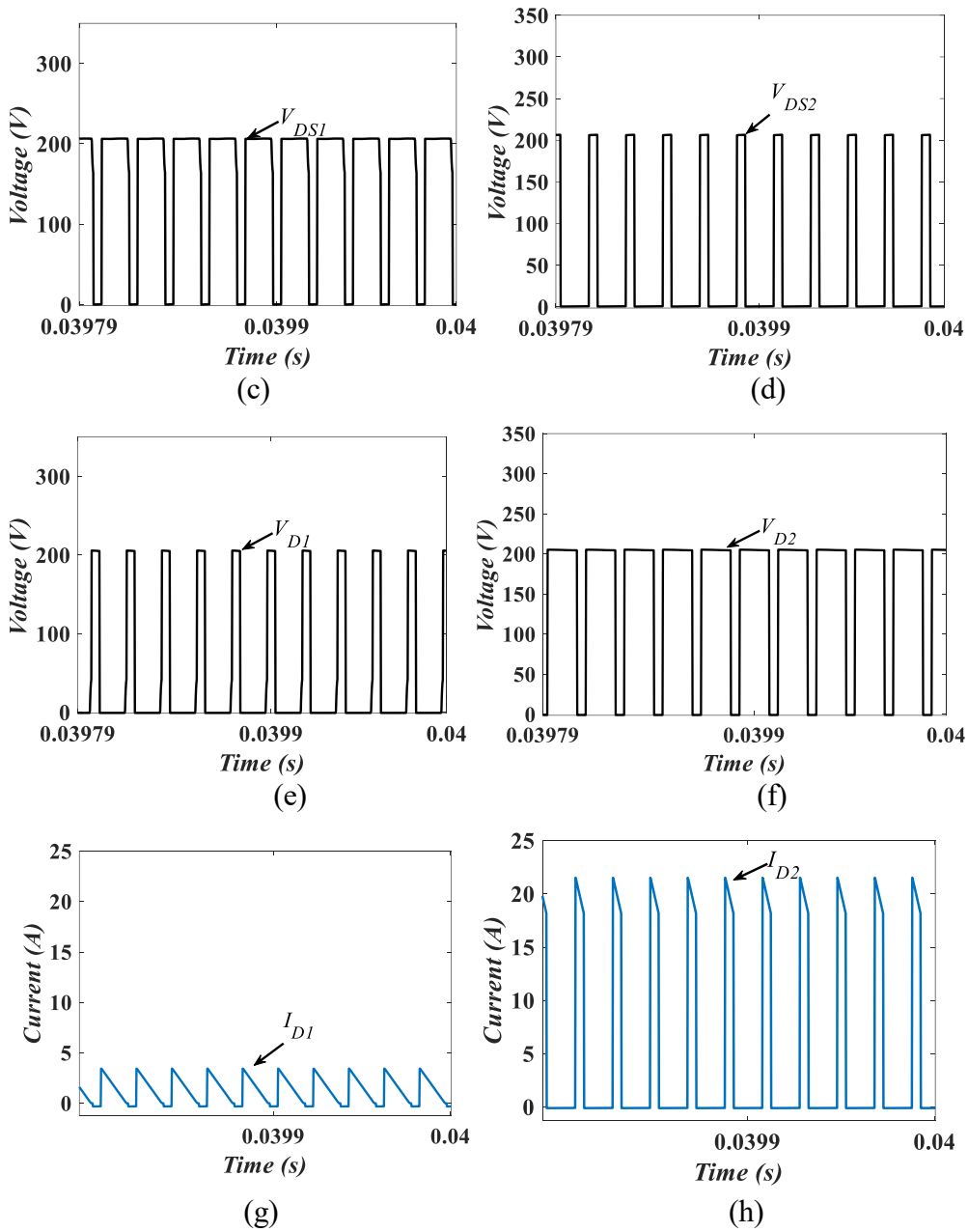

Fig. 2.9. (a) Current Stress on switch (S_1). (b) Current stress on switch (S_2). (c) Switch (S_1) drain-source voltage waveform. (d) Switch (S_2) drain-source voltage waveform. (e) Voltage stress across diode (D_1). (f) Voltage stress across diode (D_2). (g) Current stress diode (D_2). (h) Current stress on diode (D_1)

2.7. Experimental Results

A 400 W prototype of the proposed non-isolated coupled inductor based boost converter was built and tested to evaluate its performance. The design specification of the proposed converter is shown in Table 1. The waveforms for input voltage, output voltage and output current is shown in Fig. 2.10. An output voltage (V_{out}) of 205 V and output current (I_{out}) of 4.1 A for a resistive load of 50 Ohm is obtained using an input source (V_{in}) of 48 V and a duty ratio of 0.76 at a switching frequency (f_s) of 50 kHz. Experimental results for the input inductor current (I_{Lin}), inductor voltage (V_{Lin}) and switch drain-source voltages (V_{DS1} and V_{DS2}) across switches are shown in Fig.2.11.The frequency of the inductor current is twice the switching frequency. The voltage stress on switches is half of the output voltage. Fig. 12(a) and 12(b) show the voltage and current stresses across the diodes D_1 and D_2. Fig.2.13 shows the waveforms of the currents through switches S_1 and S_2. From Figs.2.12 and 2.13 the voltage and current stress is relatively low, this is enabled by the coupled inductor which divides the current among its branches. In Fig.2.14, the voltage and current waveforms of inductors L_1 and L_2 are illustrated. The inductor currents exhibit minimal ripple, presenting a notably smooth and continuous behavior. In Figure 2.14(a), we observe the closed-loop response of the converter. Notably, the duty ratio undergoes swift adjustments to maintain a steady output voltage of 205 V, effectively responding to a step change in input voltage. Furthermore, Figure 2.14(b) showcases the converter's performance in the face of a step change in load from 200 Ω to 300 Ω.

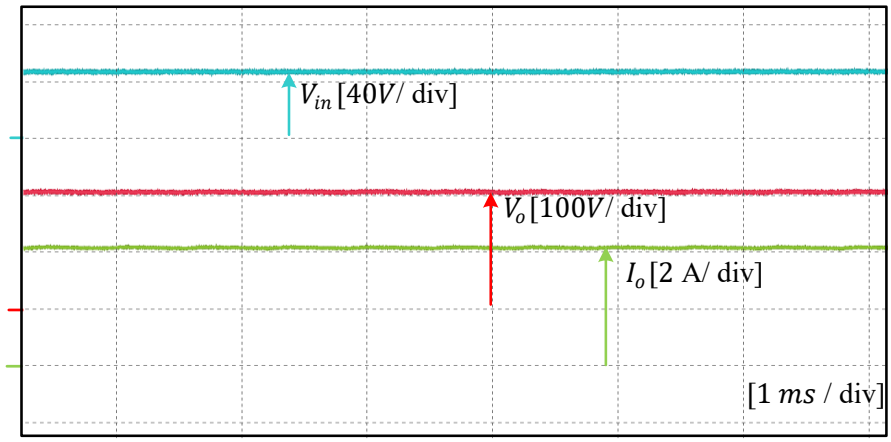

Fig. 2.10. Experimental results of input vs output voltages and output current.

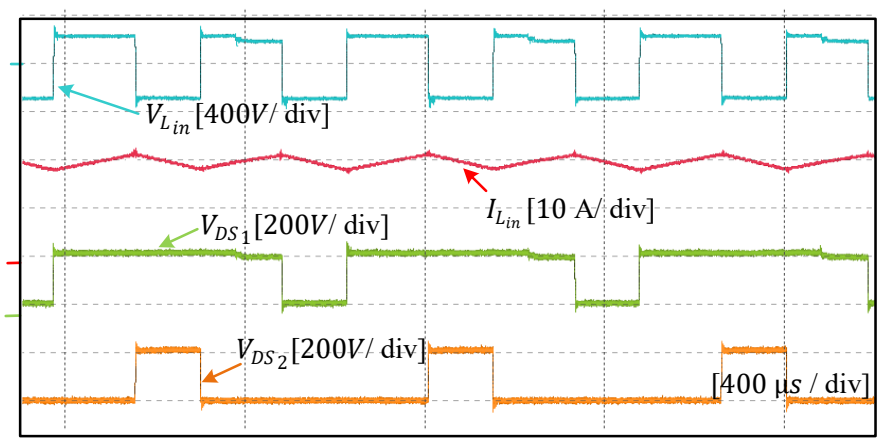

Fig. 2.11. Input inductor voltage and current, switch drain-source voltages of S_1 and S_2.

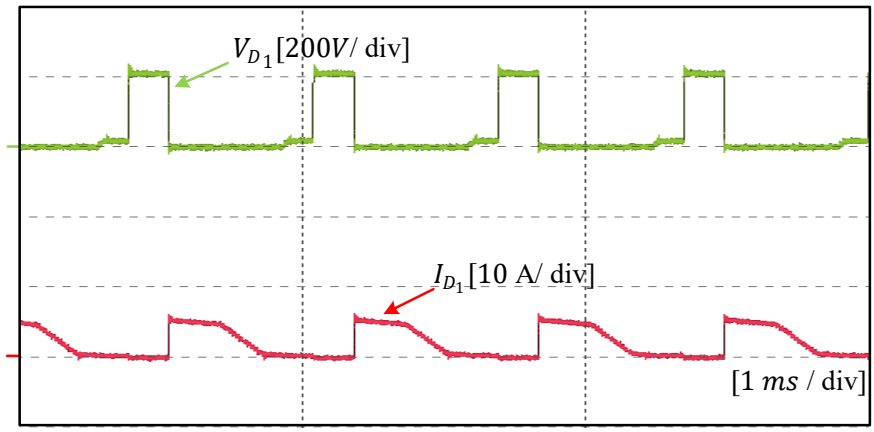

(a)

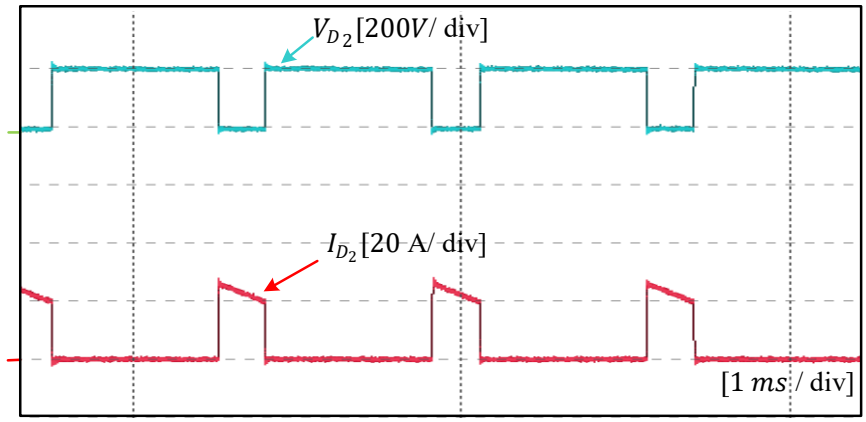

(b)

Fig. 2.12. (a) Voltage and current stress across diode $D1$. (b) Voltage and current stress on diode D_2.

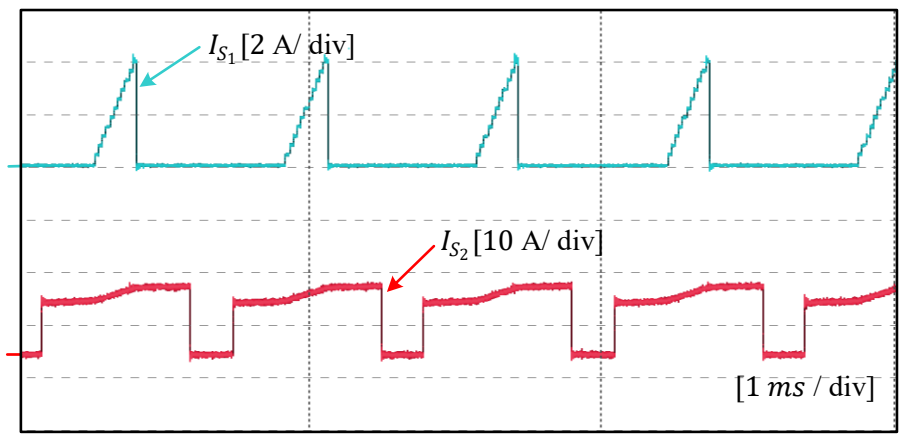

Fig. 2.13. Waveforms of current stress on switches S_1 and S_2.

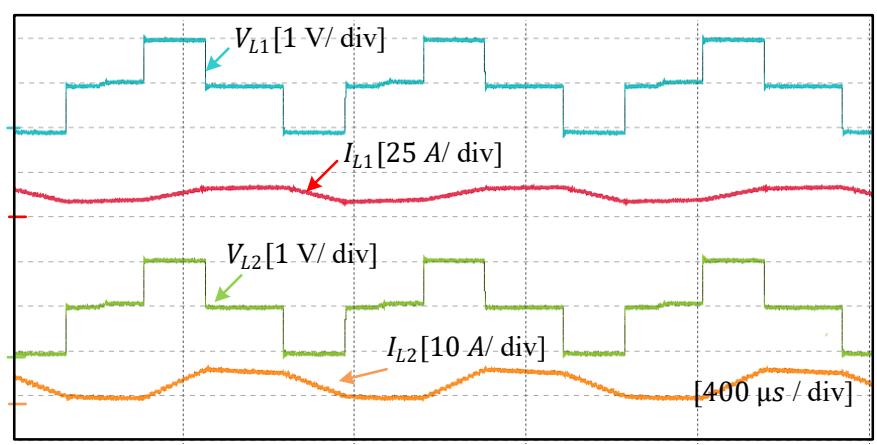

Fig. 2.14. Experimental results of inductor voltages and currents of $L1$ and $L2$.

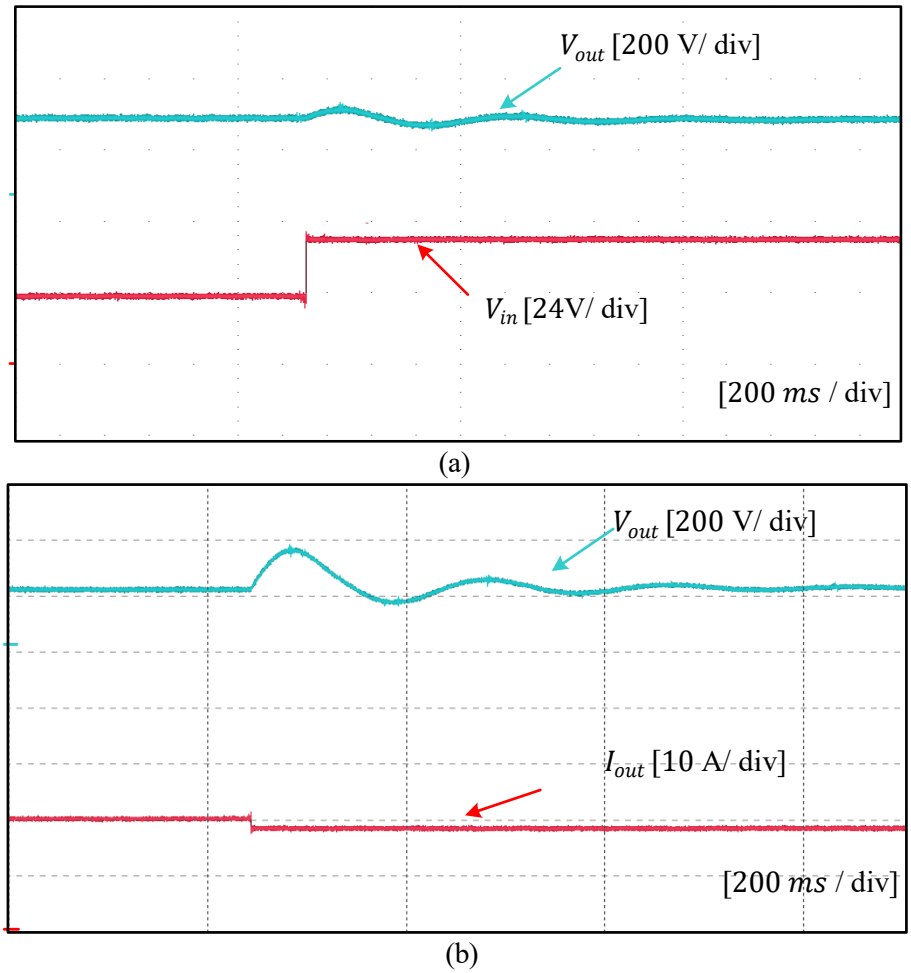

Fig. 2.15. Experimental results of converter with closed loop control. (a) Step input voltage change (b) step output load change

2.8. Conclusion

This paper introduces a novel family of bidirectional DC-DC converters employing coupled inductors with interleaved PWM scheme. The proposed converters double the effective switching frequency of the input inductors, and enable the selection of a compact filter inductor. This increase in switching frequency not only allows for smaller-sized filter inductors but also results in elevated voltage levels and reduced voltage magnitude across the

input inductors. Additionally, the proposed converters exhibit the advantage of eliminating shoot-through and reverse recovery issues associated with MOSFETs body diodes. Furthermore, it effectively maintains low voltage and current stress on both the diodes and semiconductor devices, all while establishing a common ground between the power source and the load.

References

[1] M. Forouzesh, Y. P. Siwakoti, S. A. Gorji, F. Blaabjerg, and B. Lehman, " Step-Up DC–DC Converters: A Comprehensive Review of Voltage-Boosting Techniq ues, Topologies, and Applications," *IEEE Trans. Power Electron.*, vol. 32, no. 12, p p. 9143–9178, Dec. 2017, doi: 10.1109/TPEL.2017.2652318.

[2] A. E. Khosroshahi, A. Mohammadpour Shotorbani, H. Dadashzadeh, A. Fara khor, and L. Wang, "A New Coupled Inductor-Based High Step-Up DC-DC Convert er for PV Applications," in *2019 20th Workshop on Control and Modeling for Powe r Electronics (COMPEL)*, Toronto, ON, Canada: IEEE, Jun. 2019, pp. 1–7. doi: 10.1 109/COMPEL.2019.8769630.

[3] A. P. Kumar, V. V. S. K. Bhajana, and P. Drabek, "A novel ZCS interleav ed bidirectional buck-boost DC-DC converter for energy storage applications," in *201 6 ELEKTRO*, Strbske Pleso, High Tatras, Slovakia: IEEE, May 2016, pp. 180–185. d oi: 10.1109/ELEKTRO.2016.7512061.

[4] "IET Power Electronics - 2020 - Maroti - High step-up single switch quadr atic modified SEPIC converter for DC microgrid.pdf."

[5] A. A. Khan, Honnyong Cha, and H. F. Ahmed, "A family of high efficienc y bidirectional DC-DC converters using switching cell structure," in *2016 IEEE 8th I nternational Power Electronics and Motion Control Conference (IPEMC-ECCE Asia)*, Hefei, China: IEEE, May 2016, pp. 1177–1183. doi: 10.1109/IPEMC.2016.7512455.

[6] S. Esmaeili, M. Shekari, M. Rasouli, S. Hasanpour, A. A. Khan, and H. Ha fezi, "High Gain Magnetically Coupled Single Switch Quadratic Modified SEPIC DC -DC Converter," *IEEE Trans. Ind. Appl.*, vol. 59, no. 3, pp. 3593–3604, May 2023, doi: 10.1109/TIA.2023.3250405.

[7] K. Zaoskoufis and E. C. Tatakis, “An Improved Boost-Based dc/dc Converte r With High-Voltage Step-Up Ratio for DC Microgrids,” *IEEE J. Emerg. Sel. Top. Power Electron.*, vol. 9, no. 2, pp. 1837–1853, Apr. 2021, doi: 10.1109/JESTPE.2020 .2981018.

[8] O. C. Onar, J. Kobayashi, D. C. Erb, and A. Khaligh, “A Bidirectional Hig h-Power-Quality Grid Interface With a Novel Bidirectional Noninverted Buck–Boost Converter for PHEVs,” *IEEE Trans. Veh. Technol.*, vol. 61, no. 5, pp. 2018–2032, J un. 2012, doi: 10.1109/TVT.2012.2192459.

[9] D. M. Huynh, Y. Ito, S. Aso, K. Kato, and K. Teraoka, “New Concept of the DC-DC Converter Circuit Applied for the Small Capacity Uninterruptible Power Supply,” in *2018 International Power Electronics Conference (IPEC-Niigata 2018 -E CCE Asia)*, Niigata: IEEE, May 2018, pp. 3086–3091. doi: 10.23919/IPEC.2018.8507 821.

[10] R. T. Naayagi, A. J. Forsyth, and R. Shuttleworth, “High-Power Bidirectiona l DC–DC Converter for Aerospace Applications,” *IEEE Trans. Power Electron.*, vol. 27, no. 11, pp. 4366–4379, Nov. 2012, doi: 10.1109/TPEL.2012.2184771.

[11] Sri Revathi B and M. Prabhakar, “High gain high power non-isolated DC-D C converter for renewable energy applications,” in *2014 IEEE 2nd International Conf erence on Electrical Energy Systems (ICEES)*, Chennai, India: IEEE, Jan. 2014, pp. 229–234. doi: 10.1109/ICEES.2014.6924173.

[12] K. V. G. Raghavendra *et al.*, “A Comprehensive Review of DC–DC Conver ter Topologies and Modulation Strategies with Recent Advances in Solar Photovoltaic Systems,” *Electronics*, vol. 9, no. 1, p. 31, Dec. 2019, doi: 10.3390/electronics90100 31.

[13] B. Mangu, S. Akshatha, D. Suryanarayana, and B. G. Fernandes, “Grid-Con

nected PV-Wind-Battery-Based Multi-Input Transformer-Coupled Bidirectional DC-DC Converter for Household Applications," *IEEE J. Emerg. Sel. Top. Power Electron.*, v ol. 4, no. 3, pp. 1086–1095, Sep. 2016, doi: 10.1109/JESTPE.2016.2544789.

[14] Shih-Kuen Changchien, Tsorng-Juu Liang, Jiann-Fuh Chen, and Lung-Sheng Yang, "Novel High Step-Up DC–DC Converter for Fuel Cell Energy Conversion Sys tem," *IEEE Trans. Ind. Electron.*, vol. 57, no. 6, pp. 2007–2017, Jun. 2010, doi: 10. 1109/TIE.2009.2026364.

[15] K. Tytelmaier, O. Husev, O. Veligorskyi, and R. Yershov, "A review of no n-isolated bidirectional dc-dc converters for energy storage systems," in *2016 II Inter national Young Scientists Forum on Applied Physics and Engineering (YSF)*, Kharkiv, Ukraine: IEEE, Oct. 2016, pp. 22–28. doi: 10.1109/YSF.2016.7753752.

[16] "IET Power Electronics - 2014 - Chao - Bidirectional DC DC soft-switchin g converter for stand-alone photovoltaic power (1).pdf."

[17] Y. Du, X. Zhou, S. Bai, S. Lukic, and A. Huang, "Review of non-isolated bi-directional DC-DC converters for plug-in hybrid electric vehicle charge station app lication at municipal parking decks," in *2010 Twenty-Fifth Annual IEEE Applied Po wer Electronics Conference and Exposition (APEC)*, Palm Springs, CA, USA: IEEE, Feb. 2010, pp. 1145–1151. doi: 10.1109/APEC.2010.5433359.

[18] Netaji Subhas University of Technology and A. Singh, "High Voltage Gain Bidirectional DC-DC Converters for Supercapacitor Assisted Electric Vehicles: A Rev iew," *CPSS Trans. Power Electron. Appl.*, vol. 7, no. 4, pp. 386–398, Dec. 2022, do i: 10.24295/CPSSTPEA.2022.00035.

[19] P. H. Feretti, F. L. Tofoli, and E. R. Ribeiro, "Family of Non-Isolated High Step-Up DC–DC Converters Based on the Multi-State Switching Cell," *IEEE J. Em erg. Sel. Top. Power Electron.*, vol. 10, no. 5, pp. 5882–5893, Oct. 2022, doi: 10.11

09/JESTPE.2022.3160280.

[20] A. A. Khan, H. Cha, and H. F. Ahmed, “High-Efficiency Single-Phase AC–AC Converters Without Commutation Problem,” *IEEE Trans. Power Electron.*, vol. 3 1, no. 8, pp. 5655–5665, Aug. 2016, doi: 10.1109/TPEL.2015.2494605.

[21] A. A. Khan, H. Cha, and H.-G. Kim, “Magnetic Integration of Discrete-Cou pled Inductors in Single-Phase Direct PWM AC–AC Converters,” *IEEE Tran s. Power Electron.*, vol. 31, no. 3, pp. 2129–2138, Mar. 2016, doi: 10.1109/TPEL.20 15.2427455.

[22] A. A. Khan, H. Cha, H. F. Ahmed, and H.-G. Kim, “Elimination of Filter Inductor in Switching Cell AC–AC Converters Using Magnetic Integration,” *IEEE Tr ans. Power Electron.*, vol. 31, no. 9, pp. 6317–6326, Sep. 2016, doi: 10.1109/TPEL. 2015.2501313.

[23] L. Saro, K. Dierberger, and R. Redl, “High-voltage MOSFET behavior in so ft-switching converters: analysis and reliability improvements,” in *INTELEC - Twentie th International Telecommunications Energy Conference (Cat. No.98CH36263)*, San F rancisco, CA, USA: IEEE, 1999, pp. 30–40. doi: 10.1109/INTLEC.1998.793474.

[24] Xudong Huang, Huijie Yu, Jih-Sheng Lai, A. R. Hefner, and D. W. Bernin g, “Characterization of paralleled super junction MOSFET devices under hardand soft -switching conditions,” in *2001 IEEE 32nd Annual Power Electronics Specialists Con ference (IEEE Cat. No.01CH37230)*, Vancouver, BC, Canada: IEEE, 2001, pp. 2145–2150. doi: 10.1109/PESC.2001.954437.

[25] G.-R. Zhu, S.-C. Tan, Y. Chen, and C. K. Tse, “Mitigation of Low-Frequen cy Current Ripple in Fuel-Cell Inverter Systems Through Waveform Control,” *IEEE Trans. Power Electron.*, vol. 28, no. 2, pp. 779–792, Feb. 2013, doi: 10.1109/TPEL. 2012.2205407.

[26] A. Abrishamifar, S. Samadi, and A. Ale Ahmad, “Low-frequency current rip ple reduction in front-end boost converter with single-phase inverter load,” *IET Powe r Electron.*, vol. 5, no. 9, pp. 1676–1683, Nov. 2012, doi: 10.1049/iet-pel.2011.0470.

[27] Po-Wa Lee, Yim-Shu Lee, D. K. W. Cheng, and Xiu-Cheng Liu, “Steady-st ate analysis of an interleaved boost converter with coupled inductors,” *IEEE Trans. I nd. Electron.*, vol. 47, no. 4, pp. 787–795, Aug. 2000, doi: 10.1109/41.857959.

[28] Pit-Leong Wong, Peng Xu, P. Yang, and F. C. Lee, “Performance improve ments of interleaving VRMs with coupling inductors,” *IEEE Trans. Power Electron.*, vol. 16, no. 4, pp. 499–507, Jul. 2001, doi: 10.1109/63.931059.

[29] M. Pavlovsky, G. Guidi, and A. Kawamura, “Assessment of Coupled and In dependent Phase Designs of Interleaved Multiphase Buck/Boost DC–DC Converter fo r EV Power Train,” *IEEE Trans. Power Electron.*, vol. 29, no. 6, pp. 2693–2704, Ju n. 2014, doi: 10.1109/TPEL.2013.2273976.

[30] W. C. Leal, M. O. Godinho, R. F. Bastos, C. R. De Aguiar, G. H. F. Fuz ato, and R. Q. Machado, “Cascaded Interleaved DC–DC Converter for a Bidirectiona l Electric Vehicle Charging Station,” *IEEE Trans. Ind. Electron.*, vol. 71, no. 4, pp. 3708–3717, Apr. 2024, doi: 10.1109/TIE.2023.3273281.

Chapter III
A Novel Non-Isolated Bidirectional DC-DC Converter with improved current ripples for Low voltage on-board Charging

Preface

A version of this section of the manuscript chapter has been accepted and published in MDPI Energies. I, Jamil M Khan the primary author of this paper. The research is supervised by my supervisor Dr. Ashraf Ali Khan and reviewed by my co-supervisor Dr. Mohsin Jamil. All authors have read and agreed to the published version of the manuscript.

Abstract

This paper presents a novel single-phase non-isolated bidirectional buck converter topology. The proposed converter uses a basic switching cell structure with a coupled inductor and an interleaving switching scheme. This article addresses a crucial challenge in bidirectional DC-DC conversion by prioritizing reducing output current ripples and minimizing filter inductor size. The employed method includes using MOSFETs with fast recovery diodes to mitigate reverse recovery and body diode losses. Furthermore, the optimization of the switching frequency of the output inductor to be twice the actual switching frequency contributes to reducing the component size of the converter. The coupled inductor also helps to reduce stress on components by distributing currents among its legs. The experimental result demonstrates the proposed converter has a very low ripple current as compared to the conventional converter. The low current ripples and smaller filter inductor size enabled by high-frequency operation have improved the efficiency and size of the converter. A common ground between input and output terminals ensures robust performance without common mode current concerns. Overall, the proposed converter represents a significant improvement in DC-DC converters, promising enhanced efficiency, reliability, and compactness in bidirectional DC-DC conversion systems. In order to verify the performance of the proposed converter, a 460-W buck converter prototype was built and tested.

3.1. Introduction

The increase in use of fossil fuels has significantly increased greenhouse gas emissions. These emissions are major cause of global warming. Therefore, sourcing the world's energy needs from clean and renewable energy sources is inevitable. These renewable sources are environmentally sustainable and align with the 2030 Sustainable Development Goals (SDGs) [1].

Renewable energy sources such as photovoltaics, wind power generation, and fuel cells provide a stable voltage to a DC bus through DC-DC converters [2]. These DC-DC converters are further used to charge batteries. DC-DC converters can be categorized into unidirectional and bidirectional. Unidirectional converters allow the flow of current only in one direction while bidirectional converters allow current flow in both directions, enabling the use of a single converter for both energy transfer and storage applications [3].

Bidirectional DC-DC converters (BDCs) play a pivotal role across various applications such as aerospace power systems, energy storage systems (ESS) in DC micro-grids [4], and electric vehicles (EVs). As already discussed in existing literature [4], [5], BDCs store generated energy in batteries and in time of need, these converters enable energy transfer from batteries to load. The bidirectional operation of these converters is essential, allowing them to transfer energy in both directions while ensuring voltage stability and efficiency. Moreover, bidirectional converters are integral to electric drive systems, particularly in electric transportation [6], where they fulfill the dual function of stepping up voltage during power delivery from the source to the motor and stepping down voltage during regenerative braking.

Bidirectional DC-DC converters (BDCs) can be further classified into isolated and non-isolated converters. Isolated converters have electrical isolation for safety, but they can be bulky and costly due to the use of transformers, and they also suffer from high leakage inductance [8]. Non-isolated converters lack galvanic isolation but offer higher efficiency,

compact size, and lower cost, making them preferable in many applications [7]. The conventional non-isolated buck/boost bidirectional DC-DC converters are famous for their simple structure and affordability. However, circuit parasitic parameters and the requirement for an extreme duty ratio limit its maximum achievable voltage gain. Additionally, the converter experiences high-voltage stress [8]. These converters also encounter a common issue of high ripple current on the low-voltage (LV) side. This causes the performance of BDC applications involving ESS as the large ripple current negatively impacts battery performance and lifespan [9].

Several conversion techniques are used in BDCs, including multilevel techniques [7], [10], cascaded techniques [11], [12], voltage multiplier [13], switched-inductor, switched-capacitor [14], [15], and coupled-inductor [2], [12], [16].The multilevel technique improves the voltage conversion ratio and reduces voltage stresses on power switches. However, this method increases the number of switches and complexity in control. Cascaded structures reduce high voltage stresses on power switches but result in lower power density and increased converter cost. Similarly, a switch inductor can lead to low switch stress and high gain, but the difference between the low voltage side (LVS) and high voltage side(HVS) can lead to EMI problems [14]. The couple-inductor topologies can increase the gain, but the leakage inductance issue can produce high voltage spikes on switches and may require additional snubber circuitry [16].

One common issue in the above-mentioned BDCs, is the presence of significant ripple current on the LVS. This ripple current is a problem for Battery Energy Storage Systems (BESS), which are sensitive to such fluctuations. Excessive ripple current can shorten the lifespan of the BESS [18], [19]. To minimize current ripples in converters, several techniques can be used as discussed below:

- One approach is to increase the inductance of the inductors. This reduces current

ripple but it can slow down the dynamic response, cost, and size of the converter due to the larger inductor size [20].

- **U**sing a large capacitor can solve the ripple issues, but it increases the size and cost of the converter.
- Increasing the switching frequency can help reduce ripple current and allow for smaller inductors. However, the switching frequency increase is constrained by gate drive circuit limitations, switching losses, and electromagnetic compliance requirements.
- Implementing DCM in converters can lower inductor size. However, the higher inductor current in DCM mode increases switch stress, leading to increased power loss.
- Inductor ripple can be reduced by employing the interleaving technique, [21]. Although effective, this method increases the number of switches and inductors, thereby complicating control and increasing converter cost.
- Utilizing cascaded converters with phase shifts can also decrease inductor ripples [19]. However, this approach may raise complexity and cost due to increase in component count. The converter must also operate within a fixed duty cycle.

Each technique for reducing ripple current in bidirectional DC-DC converters involves trade-offs in performance, complexity, and cost. The choice depends on specific design requirements and constraints. The recent advancement in interleaving DC-DC converter have made it an excellent choice for increase power density and higher efficiency. [22] Discussed design and modeling of a DC-DC converter using interleaving technique and by exploiting the quasi-saturated inductor it has reduced the size of the inductor. Similarly,[23] has devised a more robust nonlinear control technique for an interleaved converter against parameter variations.

While research has examined various non-isolated bidirectional converters, few have focused on using a coupled inductor in a non-isolated DC-DC converter, as shown in Figure.1 of our design. This concept, however, has been applied in DC-AC converters[24], [25], as well as in AC-AC applications[26]. This observation highlights the versatility and widespread applicability of the mentioned coupled inductor with cell structure topology across various domains within power electronics.

This study addresses the challenge of optimizing voltage reduction while maintaining efficiency and compactness in bidirectional buck converters. We propose a novel design for onboard charging and battery energy storage systems (BESS), employing coupled inductors and an interleaved PWM scheme for improved efficiency, reduced size, and simplified control. The proposed non-isolated BDC has the following main characteristics:

- Low output ripple current
- The inductor operates at twice the switching frequency
- Reduced inductor size
- low voltage stresses on power switches
- Common ground between LVS and HVS.
- No additional RC snubbers circuit is required.
- No shoot-through or dead time issue.
- Less component count and reduced overall size.

The subsequent sections of this paper delve into the proposed buck converter topolo-gy, proposed switching (Section II) and modes of operation (Section III), , ripple current analysis and component selection (Section IV), stress and power loss analysis (Section V) experimental results (Section V), and discussion and conclusion in the last section.

3.2. Proposed Buck Converter Topology and Switching Scheme

3.2.1. Proposed Topology

The proposed circuit of a non-isolated bidirectional buck DC-DC converter is shown in Fig.3.1. This converter employs two active switches (S1, S2) and two independent diodes (D1, D2), a coupled inductor (CL) which is specifically chosen with a coupling factor of k=1, an output filter inductor (Lout) and capacitor (Co). The input source voltage is denoted by Vin, and Vo represents the output voltage. The switches operate at a switching frequency of 50 kHz. This circuit configuration offers several benefits. This converter demonstrates reduced output filter inductor (Lout) requirements as it experiences double switching frequency and low voltage stress. Additionally, by utilizing a fundamental switching cell structure, the proposed circuit eliminates the shoot-through and dead-time concerns. Moreover, the circuit features a shared ground, making it well-suited for applications in renewable energies.

3.2.2. Proposed Topology

The proposed modulating signals designed for driving the switches are shown in Figure.3.2. The Suggested converter employs an interleaved PWM switching scheme depicted in Fig. 3.2. The switching signals are generated by comparing a DC reference voltage with two 50 kHz triangular waves (V_{tri1}, V_{tri2}), which are out of phase by 180 degrees. The output signal for triangular wave (V_{tri1}) is fed to a NOT gate to operate Switch S_1. This configuration encompasses both dead time and overlap time operation modes. The duty cycle as denoted by D, signifies the duration during which S_1 is in the "ON" state within a single switching period (Ts).

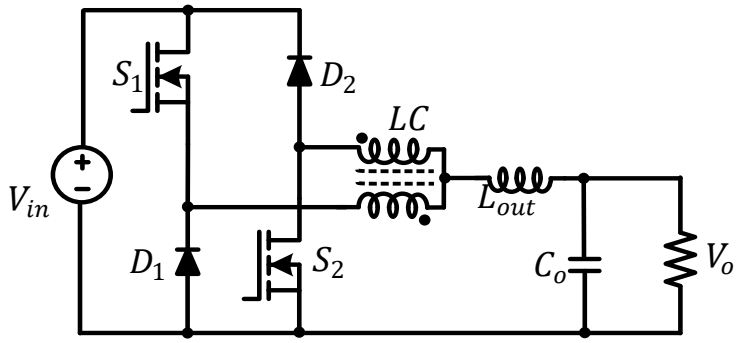

Fig.3.1. Proposed DC-DC buck converter.

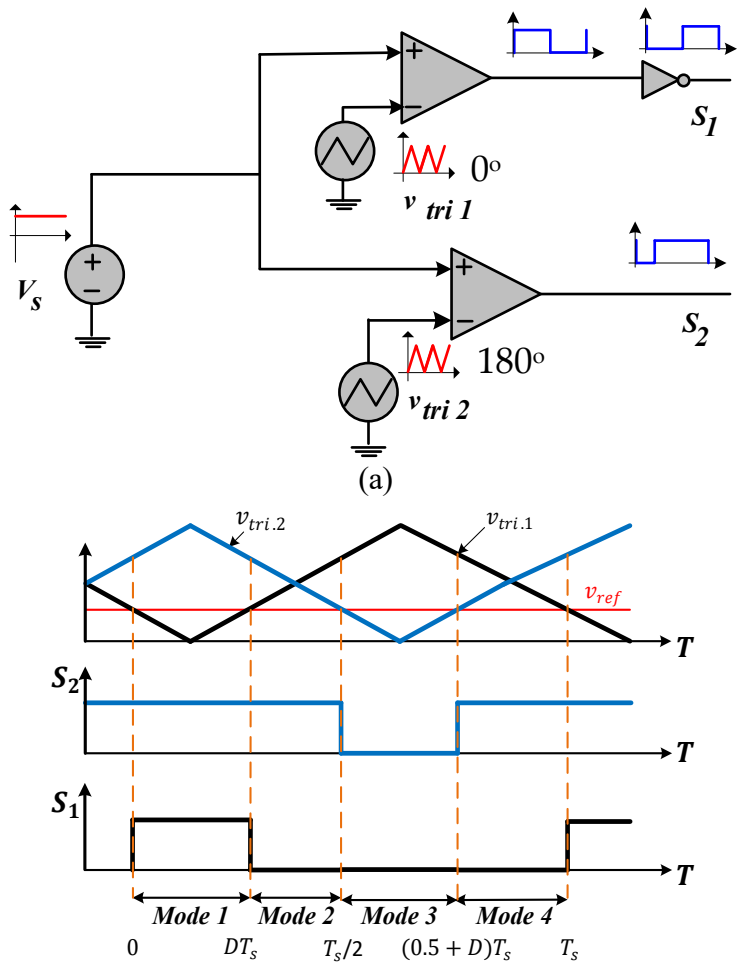

Fig.3.2. Proposed PWM scheme (a) switching signal generation. (b) Switching waveform.

3.3. Operation Modes

The suggested converter operates in four different modes as shown in the Fig 3.3. The system comprises two current components; the output inductor current (I_{out}) and the common mode current (I_{cm}), often referred to as circulating current. In this topology, it is assumed that the coupled inductors are identical, and the coupling coefficient, *K* is deliberately set to *1*, signifying tight coupling. The operations mode are discussed below for duty ratio greater and less than zero (D<0, D>0).

3.3.1. Operation Mode For D<0

Mode I: Mode 1 is shown in Fig. 3.3(a). During this mode switches S_1 and S_2 are both turned ON, and the diodes D_1, and D_2 are reverse-biased. Output Inductor (L_{out}) is charged in this mode, and the filter capacitor C_o supplies the output voltage. The voltage and current equations are as follows:

For tight coupling, k=1 and $V_{C_o} = V_o$, and we get

$$V_{L_{out}} = \frac{V_{in}}{2} - V_o \tag{3.1}$$

$$L_{out} \frac{dI_{L_{out}}}{dt} = \frac{V_{in}}{2} - V_o \tag{3.2}$$

Similarly, the voltage across the coupled inductor is given by

$$V_{L_{out}} = L\frac{dI_{in}}{dt} \tag{3.3}$$

Where L is the inductance of L_1 and L_2.

Mode II*:* During this interval, the switch S_1 is turned OFF, and S_2 is ON, the diode D_1 is conducting the circulating current due to freewheeling action, and D_2 remains OFF. Mode 2 is shown in Fig. 3.3(b). The voltage and current equations are as follows:

$$V_{L_{out}} = -V_o \tag{3.4}$$

$$L_{out} \frac{dI_{L_{out}}}{dt} = -V_o \tag{3.5}$$

Mode III: During this interval, *S1* and *S2* are turned off and diodes D_1 and D_2 are conducting as shown in Fig. 3.3(d). The voltage and current equation are as follows

$$V_{L_{out}} = \frac{V_{in}}{2} - V_o \tag{3.6}$$

$$L_{out} \frac{dI_{L_{out}}}{dt} = \frac{V_{in}}{2} - V_o \tag{3.7}$$

Mode IV: Mode IV is shown in Figure 3.3(b). It is same as Mode II

3.3.2. Operation Mode For D>0

Mode I: As shown in Figure 3.3(a), Mode I is the same for both D<0 and D>0.

Mode II: During this interval, the switch S_1 is turned ON and S_2 is OFF, the diode D_2 is conducting the circulating current due to freewheeling action, and D_1 remains OFF. From Figure. 3.3(c) the equation for voltage and current are the same as equation (3.6) and (3.7)

Mode III: During this mode , *S1* and *S2* are turned off and diodes D_1 and D_2 are conducting as shown in Fig. 3.3(d).Mode III is same for both D>0 and D<0.

Mode IV: Mode IV is the same as Mode II as indicated in Figure 3.3(c)

The output voltage gain of the proposed buck converter can be obtained by applying the Volt-Sec balance condition on L_{out} which leads to the following equation:

$$V_o = DV_{in} \tag{3.8}$$

Equation (3.8) is the ideal gain equation of the proposed converter. This equation is similar to a conventional buck converter gain equation.

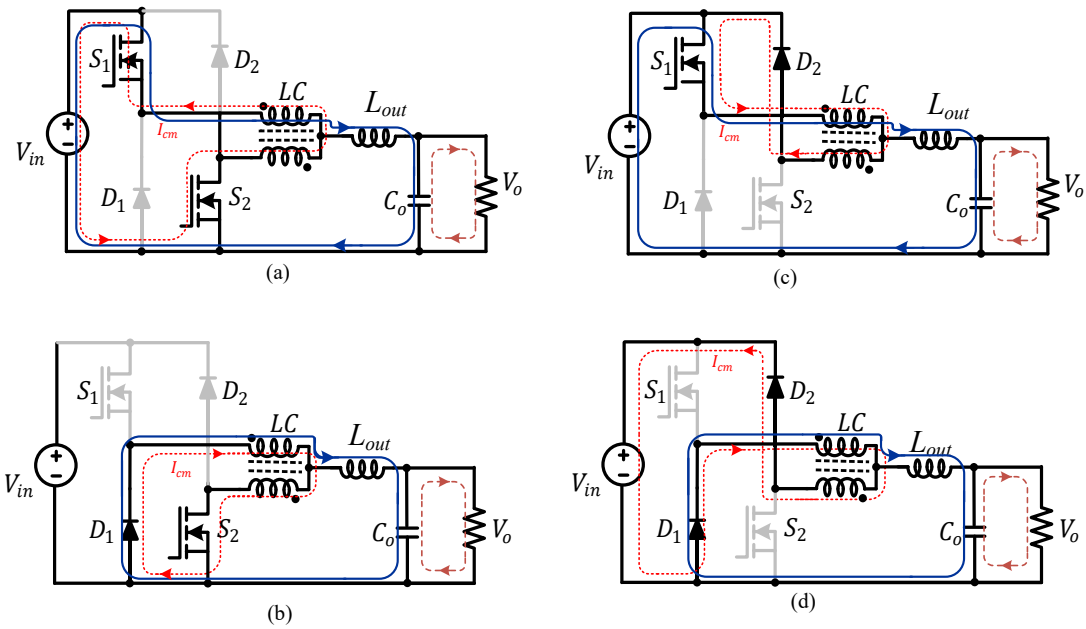

Fig. 3.3. Proposed Converter operation modes. (a) Mode 1 for D<0.5 and D>0.5. (b) Mode 2, Mode 4 for D<0.5. (c) Mode 2, Mode 4 for D>0.5. (d) Mode 3 for D<0.5 and for D>0.5.

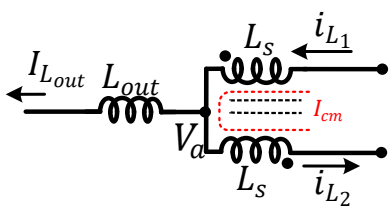

Fig. 3.4. Couple inductor and common mode current.

The non-ideal model of the proposed converter is shown in Fig. 3.5. To derive the non-ideal gain equation, different non-idealities such as equivalent series resistance (ESR) of inductor r_{la}, ESR of capacitor r_c, switch on-resistance r_{sw}, diode forward resistance r_D, Coupled inductor equivalent series resistance r_{La}, and diode forward voltage drop V_F are considered. The values of these parasitic resistances are very small in comparison to load resistance *R*. Since, a negligible current is passing through inductor of the coupled inductor L_b, therefore the ESR of this branch is not considered. The non-ideal gain equation is given

by equation (3.9)

$$V_{out} = \frac{V_{in}D}{2D\left(1 + \frac{(r_{sw} + r_{la} + r_{Lout})}{R}\right) + 2(0.5 - D)(1 + \frac{r_{Lout}}{R})} \tag{3.9}$$

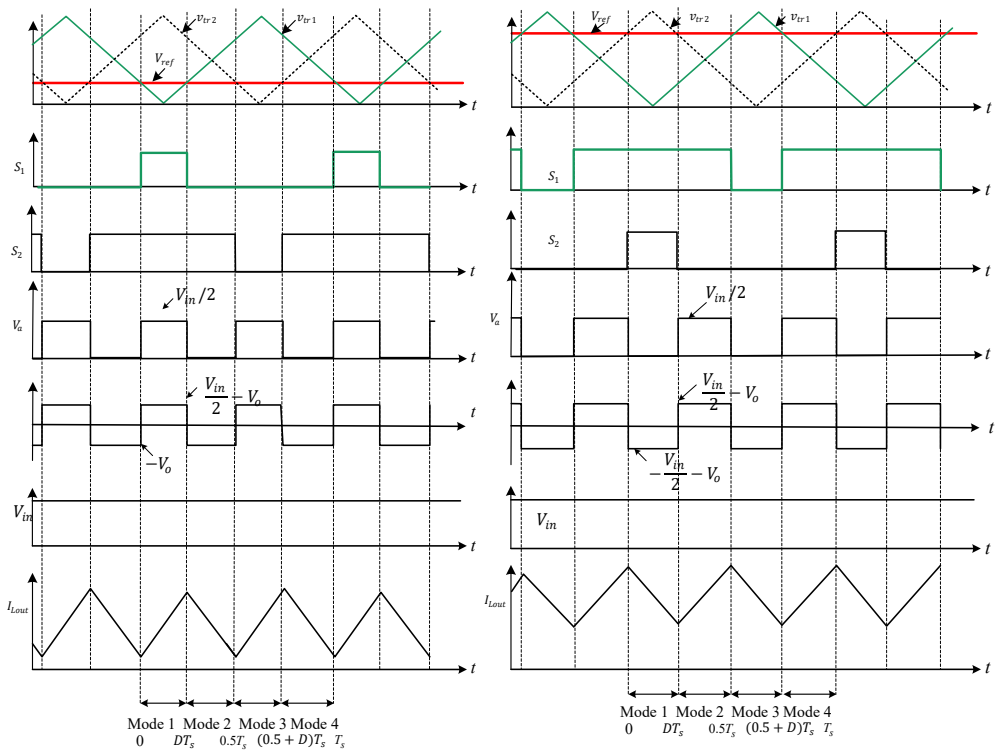

(a) (b)

Fig. 3.4. Key Simulation waveforms (a) D < 0.5 (b) D > 0.5.

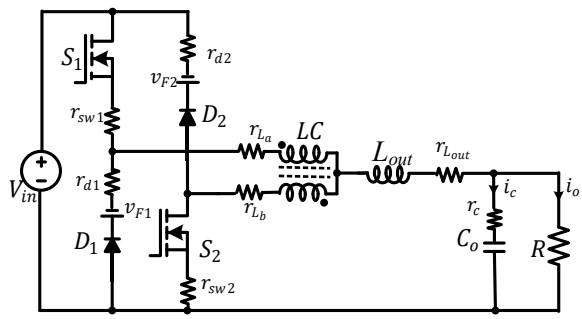

Fig. 3.5. Non-ideal model of the proposed converter.

3.4. Ripple current analysis and component selection

In this section, the current ripple magnitudes of the input and coupled inductors are discussed in this section.

3.4.1. Inductor Design

From equation (3.7) and (3.8), the input inductor equation can be derived as

$$L_{out}\frac{dI_{L_{out}}}{dt} = \frac{(V_{in} - 2V_{out})}{2} \tag{3.10}$$

From equation (3.6)

$$\begin{cases} L_{out} \geq \dfrac{(V_{in} - 2V_{in}D)DT_s}{2\Delta I} \\ L_{out} \geq \dfrac{V_{in}(D - 2D^2)}{2\Delta \mathrm{I} f_{sw}} \end{cases} \tag{3.11}$$

$\Delta \mathrm{I} = \mathrm{x}\%I_{out}$, with x% denoting the maximum permissible current ripple (10%-20%) for the inductors and $T_s = \frac{1}{f_s}$ is the switching period of the converter

$$L_{out} \geq \frac{V_{in}D(1 - 2D)}{\mathrm{x}\%I_{L_{out}}f_s} \tag{3.12}$$

Assuming that the ripple inductor current ripple ΔI_{Lout} is equal to the output ripple current ΔI_{out}, since the capacitor draws a negligible current. The output inductance equation L_{out} can be derived using (3.10) as

$$L_{out} \geq \frac{V_{in}D(1 - 2D)}{x\%I_{out}f_s} \tag{3.13}$$

The Inductor equation can be written in terms of the input voltage by assuming that the converter is lossless, i.e. $P_{out} = P_{in}$. Equation (3.11) becomes

$$L_{out} \geq \frac{{V_{in}}^2D^2(1 - 2D)}{\mathrm{x}\%P_{out}f_s} \tag{3.14}$$

3.4.2. Output Inductor Ripple

The Current ripple $\Delta I_{L_{out}}$ through the filter inductor L_{out} can be calculated from (3.11)

$$\Delta I_{L_{out}} = \frac{V_{in} D(1-2D)}{L_{out} f_s} \tag{3.15}$$

From equation (3.13), maximum ripples in the inductor current occur at D = 0.25 and $T_s = \frac{1}{f_s}$ is the switching period of the converter.

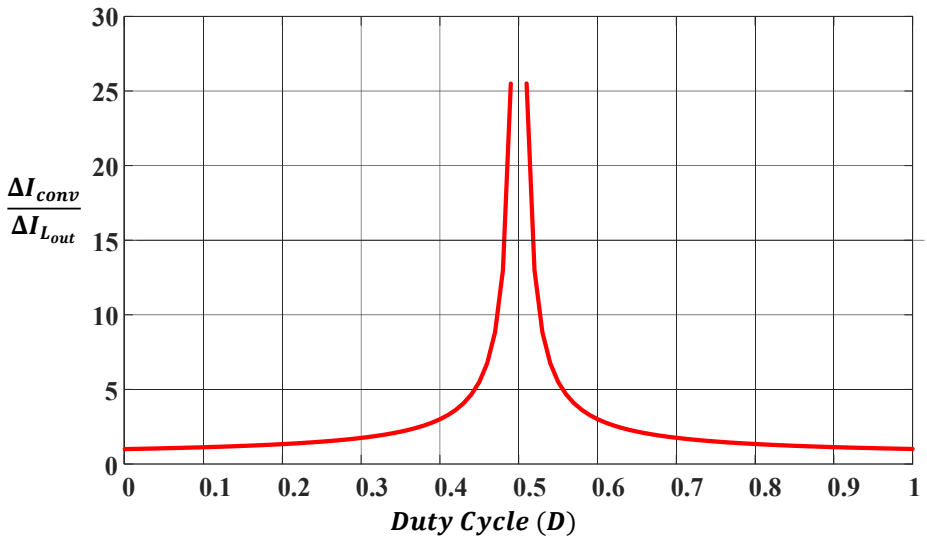

Fig. 3.6. Output current ripple comparison of the proposed and conventional buck converter.

3.4.3. Comparison of Current Ripples

The ripple current for the conventional converter can be derived as;

$$\Delta I_{conv} = \frac{(V_{in} - V_o) D T_s}{L_{conv}} \tag{3.16}$$

Using (3.15) and (3.16), the ratio of conventional versus proposed induction ripple current ($\Delta I_{conv} / \Delta I_{L_{prop}}$) can be written as;

$$\frac{\Delta I_{conv}}{\Delta I_{L_{out}}} = \left|\frac{(1-D)}{(1-2D)}\right| \tag{3.17}$$

Fig. 3.6. illustrates the current ripple ratio with variations in duty ratio *(D)* from 0 to 0.5. As depicted, the ripple current for the conventional buck converter (ΔL_{conv}) is notably larger compared to that of the proposed converter ($L_{in_{conv}}$). For example, when D = 0.47, (ΔI_{conv}) is nearly 10 times greater than the current ripples of the proposed converter ($\Delta I_{L_{out}}$). The graph clearly illustrates that the proposed converter offers very low ripple current, making it suitable for charging energy storage elements without affecting their health.

3.4.4. Couple Inductor Design

The coupled inductance using common mode current from equation (3) can be written as

$$\begin{cases} \frac{dI_{cm}}{dt} = \frac{V_{in}}{4L_s} \\ dI_{cm} = \frac{dtV_{in}}{4L_s} \end{cases} \tag{3.18}$$

$$L_s = \frac{V_{in}.DT_s}{4dI_{cm}} \tag{3.19}$$

where L_s is self-inductance of the coupled inductor.

$$L_s = L_K + L_m \tag{3.20}$$

The leakage inductance is considered very small ($L_K \approx 0$), equation (3.20) becomes

$$L_s = L_m \tag{3.21}$$

Equation (19) can be written as

$$L_m = \frac{V_{in}.DT_s}{4dI_{cm}} \tag{3.22}$$

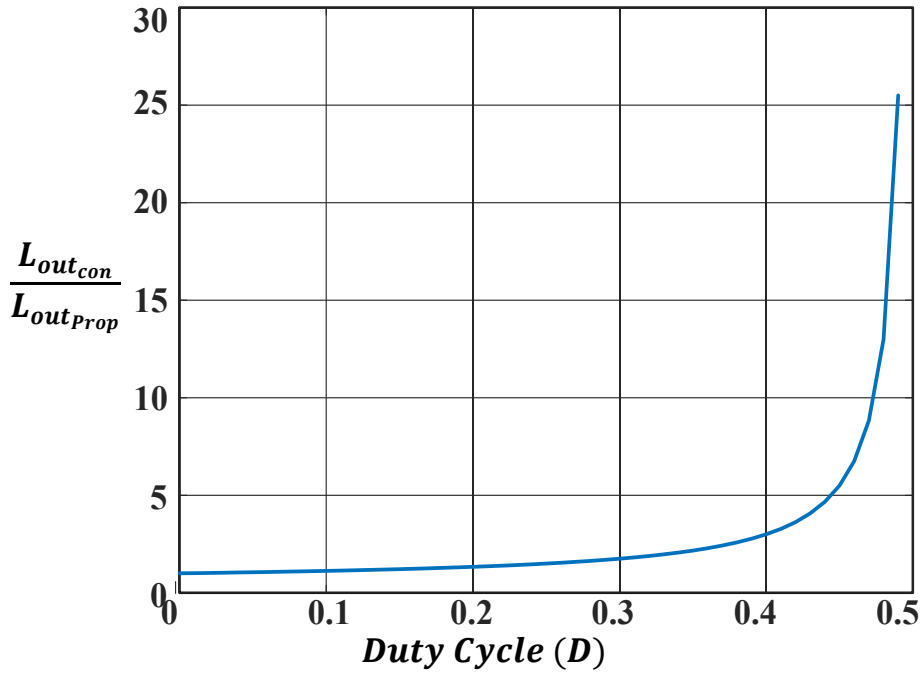

Fig. 3.7. Output inductance comparison of the conventional versus the proposed converter.

3.4.5. Output Inductor comparison

Using equation (15) and equation (16) the normalized ratio of the conventional versus proposed output inductance ($\frac{L_{out.conv}}{L_{out.prop}}$) can be derived as below.

$$\frac{L_{conv}}{L_{prop}} = \frac{(1-D)}{(1-2D)} \tag{3.23}$$

Fig. 3.7 illustrates the necessary inductance value for the conventional DC-DC converter for the same current ripple value as observed in the proposed converter, with variations in duty ratio *(D)* from 0 to 0.5. As depicted, the output inductance for the conventional C-DC converters ($L_{out.conv}$) is notably larger than that of the proposed converter ($L_{out.prop}$). For example, when D = 0.47, $L_{out.conv}$ is nearly 13.5 times the size of the proposed output inductor.

3.5. Stress and Power Loss Analysis

3.5.1. Voltage and Current Stress

Voltage stress (V_{DS_n}) across switches of the proposed converter is given below

$$V_{DS_n} = V_{in} \tag{3.24}$$

equation (3.34) Shows that the voltage stress across the switches is equal to the input voltage. Similarly, the current stress is the sum of output current ($I_{L_{out}}$) and the output inductor ripples.

$$I_{stress} = I_{L_{out}} + \quad \Delta I_{L_{out}} \tag{3.25}$$

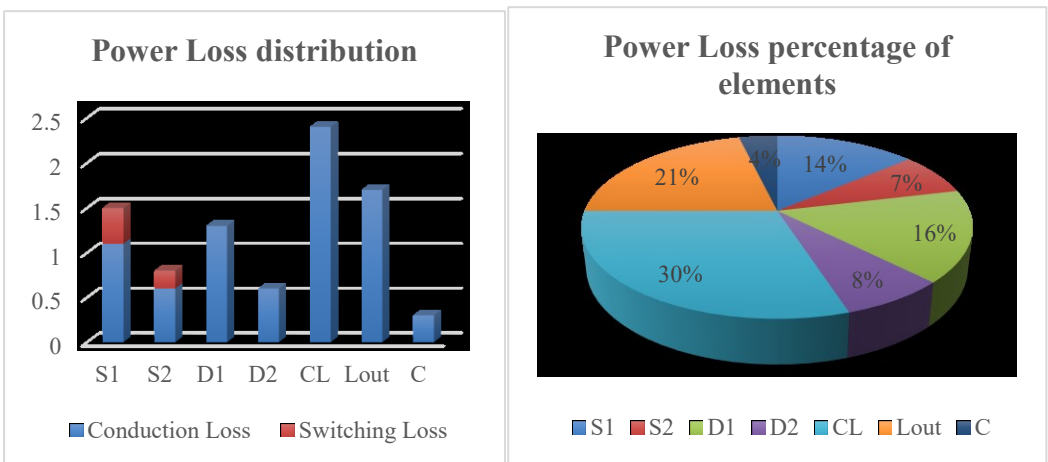

(a) (b)

Fig. 3.8. Power loss analysis. (a) Conduction and switching loss of elements. (b) Component wise percentage loss.

3.5.2. Power Loss

The major contributors to the power dissipation the proposed converter are the conduction losses of the parasitic components and switching losses of the MOSFET. The parasitic components, r_{DS_n}, r_{D_n}, V_{F_n}, r_{L_n} and r_c are the switch ON-state resistance, the

diode's forward resistance, the diode forward drop voltage, the inductor's ESR and the capacitor's ESR respectively.

The conduction loss of the switches ($P_{con_{sn}}$) can be derived as

$$P_{con_{sn}} = {I_{Sn_{rms}}}^2 . r_{DS} \tag{3.26}$$

The switching loss of the switches S_1 and S_2 ($P_{sw_{sn}}$) is given b

$$P_{sw_n} = f_s . C_{eq} . \frac{{V_{DS_n}}^2}{2} \tag{3.27}$$

where f_s is switching frequency, C_{eq} is the constant equivalent capacitance of the switch, and V_{DS_n} is the voltage stress across the switches. From equation (3.24) $V_{DS_n} = V_{in}$, (3.27) can be written as

$$P_{sw_n} = f_s . C_{eq} . \frac{{V_{in}}^2}{2} \tag{3.28}$$

Where $I_{Sn_{rms}}$ is the switch rms current, and f_s is the switching frequency. The conduction loss of the diodes ($P_{con_{Dn}}$) is due to r_{D_n} and V_{F_n}. The estimated conduction loss is

$$P_{con_{Dn}} = I_{Dn_{avg}} . V_{F_n} + {I_{Dn_{rms}}}^2 . r_{D_n} \tag{3.29}$$

The conduction losses of the inductors are estimated as

$$P_{con_{Ln}} = {I_{Ln_{rms}}}^2 . r_{L_n} \tag{3.30}$$

The conduction losses of the capacitor is given by

$$P_{con_{Cn}} = {I_{Cn_{rms}}}^2 . r_{L_n} \tag{3.31}$$

The inductors also experience core losses in their operation. The core loss inductors are given by

$$\begin{cases} P_{fe(L_{out})} = \ lm. Ac. Kfe. {B_{max}}^{\beta} \\ P_{fe(CL)} = \ lm. Ac. Kfe. {B_{max}}^{\beta} \\ P_{fe(total)} = \ P_{fe(L_{out})} + P_{fe(CL)} \end{cases} \tag{3.32}$$

Where, lm, Ac, Kfe, B_{max}, and β, represent the magnetic path length, the core's cross-sectional area, the core loss coefficient, maximum flux density, and the core loss exponent, respectively.

In the experimental works, at an output power of 460 W, the component's power loss breakdown is included to provide a clear analysis of the proposed converter, as shown in Fig. 3.8(a). Additionally, Fig. 3.8(b) illustrates the percentage power loss distribution among the switch, diodes, inductors, and capacitors.

Table 3. 1

Component specifications (Bidirictional Buck Converter)

Components	***Values***
Input voltage (V_{in})	200 V
Output voltage (V_{out})	48 V
Rated output power	460 W
MOSFET (S_1, S_2)	NTHL065N65S3HF
Switching frequency	50Khz
Diodes (D_1, D_2)	BYC30JT-600PSQ
Controller	TMS320F28335
Inductors (L_{out})	0.1 mH
Output Capacitor (C_O)	100 μF

3.6. Experimental Results and Discussion

The experimental setup was designed based on the previous analysis. The proposed converter prototype was tested at 460 W hardware prototype to verify its operations. Table I shows the electrical specifications of component to build the prototype.

The experimental results were performed with a duty ratio less than 0.5. Fig. 3.9 and Fig. 3.10 illustrate the experimental results obtained with resistive load. Fig. 3.9 (a) show the input voltage (V_{in}), output voltage (V_{out}) , output current ($I_{out.}$) and input current (I_{in}). Fig. 3.9(b) shows the voltage stress across the switches (V_{DS_1}, V_{DS_2}) and diodes (V_{D_1}, V_{D_2}).These results indicate that the voltage stress is equal to the input voltage of the proposed buck converter. Fig. 3.9(c) shows current stress across the switches and diodes.

Fig. 3.10(a) provide experimental results of the voltage stress across the switches (V_{DS_1}, V_{DS_2}) and the current through the output inductor ($I_{L_{out}}$). Fig. 3.10(b) provide expanded view of Fig. 3.10(a), it illustrates that the output inductor ($I_{L_{out}}$) frequency is twice the switching frequency resulting in to a lower ripple current. Similarly, Fig. 3.10(c) simulation results of the output inductor current ($I_{L_{out}}$) along with coupled inductor currents (I_{L_1}, I_{L_2}). Fig. 3.10(d) provide expanded view of Fig. 3.10(c).. Furthermore, Fig. 3.11(a) illustrates the Inductor current of the proposed ($I_{L_{Prop}}$) and conventional ($I_{L_{Conv}}$) converter. From Fig. 3.11(b), the zoom-in simulation results, it is evident that the current flowing through the inductor of the proposed converter for the same output voltage is very small compared to that of the conventional converter.

Fig. 3.12 shows the experimental result of the inductor's voltages of the proposed and conventional converter ($V_{L_{prop}}, V_{L_{Conv}}$). These results clearly show that the voltage across the proposed converter's inductor is minimal compared to the conventional converter. Fig. 3.13 shows the response of the change in the input voltage, when the input voltage is increased from 200V to 300V, the corresponding output voltage and current remains stable. Fig. 3.14 shows the experimental setup of the proposed converter

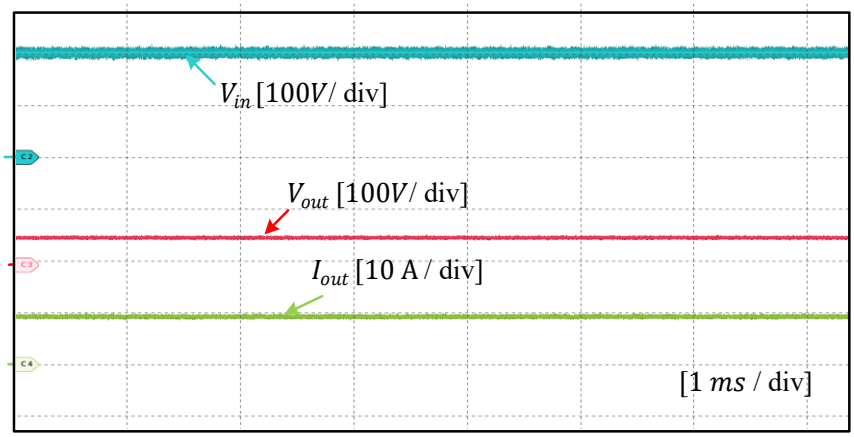

(a)

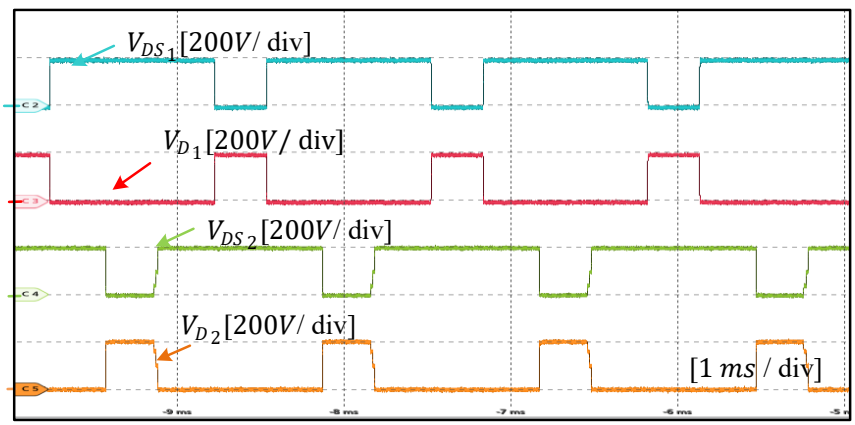

(b)

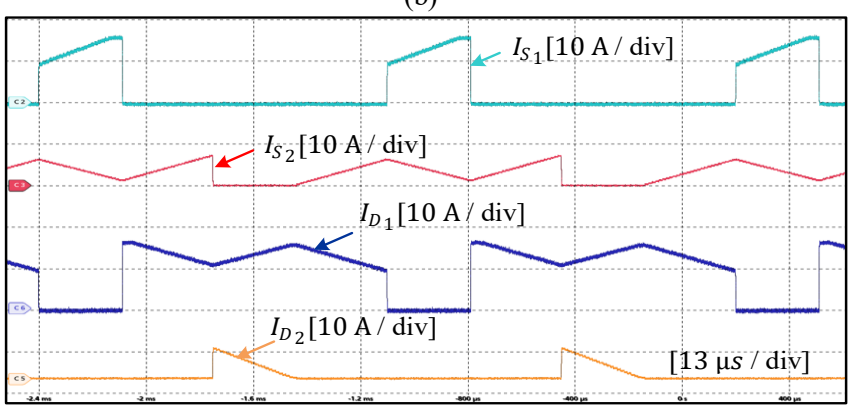

(c)

Fig. 3.9. Experimental results: (a) Show the input voltage *(V_{in}),* output voltage *(V_{out})*, output current ($I_{out.}$) and Input current ($I_{in.}$).(b) Drain-sources voltages of switches, (V_{DS_1}, V_{DS_2}) and Voltage stress across Diodes (D_1, D_2). (c) Current Stress across switches and diodes.

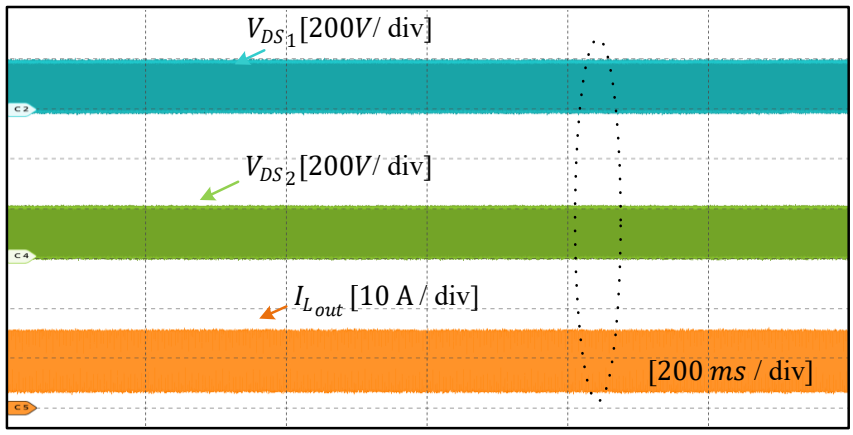
V_{DS_1}[200V/ div]
V_{DS_2}[200V/ div]
$I_{L_{out}}$ [10 A / div]
[200 ms / div]

(a)

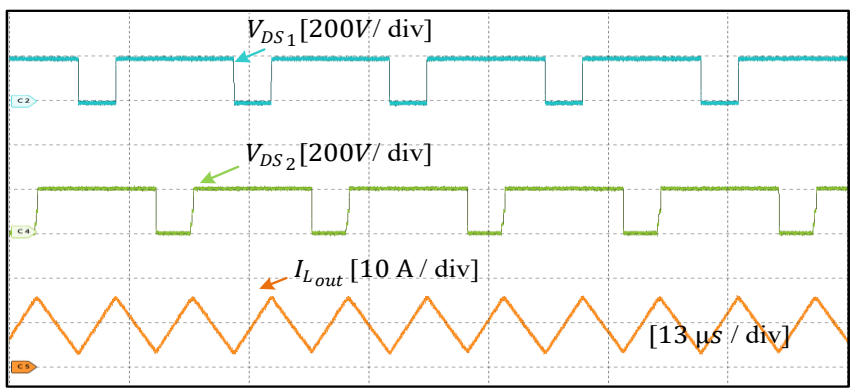
V_{DS_1}[200V/ div]
V_{DS_2}[200V/ div]
$I_{L_{out}}$ [10 A / div]
[13 µs / div]

(b)

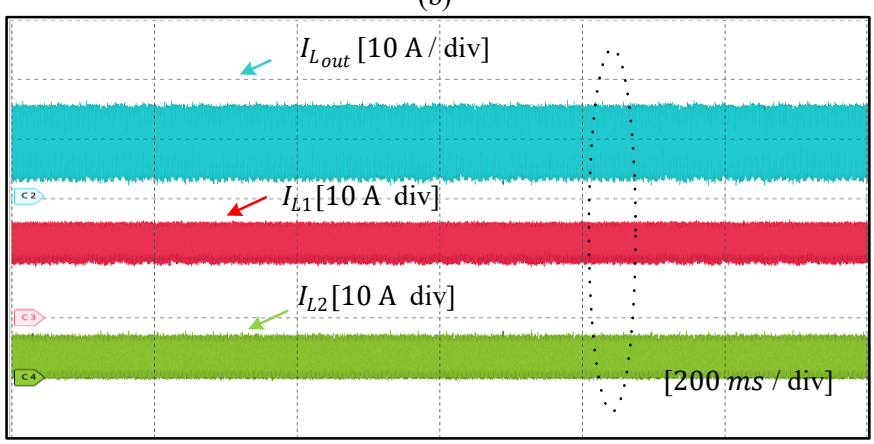
$I_{L_{out}}$ [10 A / div]
I_{L1}[10 A div]
I_{L2}[10 A div]
[200 ms / div]

(c)

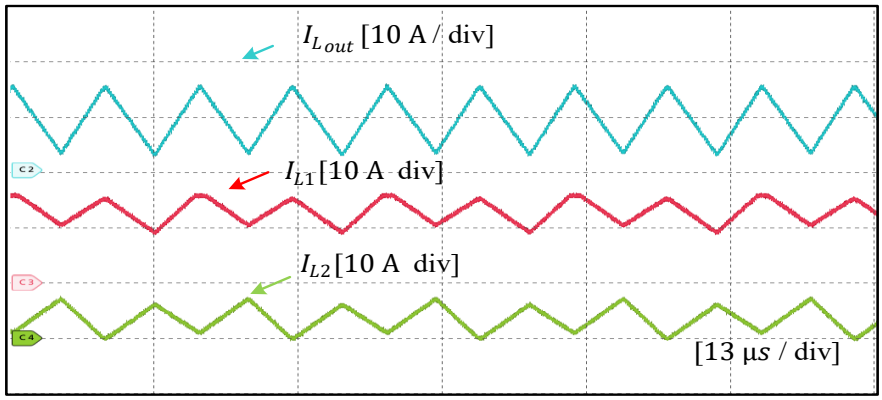

(d)

Fig. 3.10. Experimental results. (**a**) expanded results of the voltages stress V_{DS_1}, V_{DS_2}) and ($I_{L_{out}}$). (b) Zoom in simulation results of (a). (c) Expanded simulation results of $I_{L_{out}}$ and (I_{L_1}, I_{L_2}. (d) zoom in simulation results of (c).

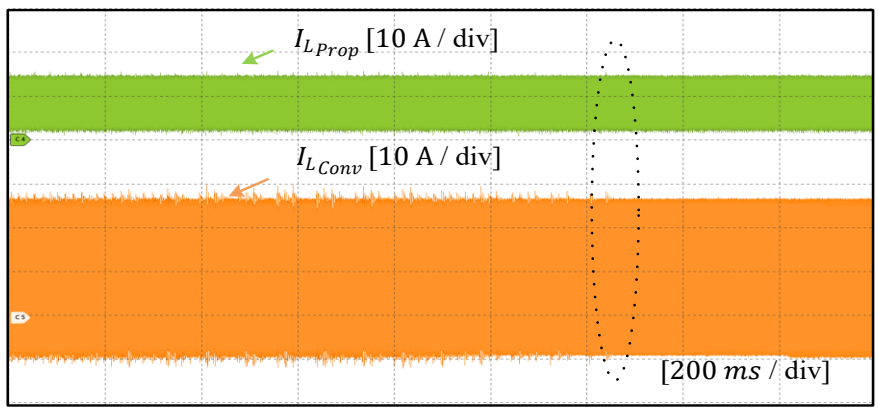

(a)

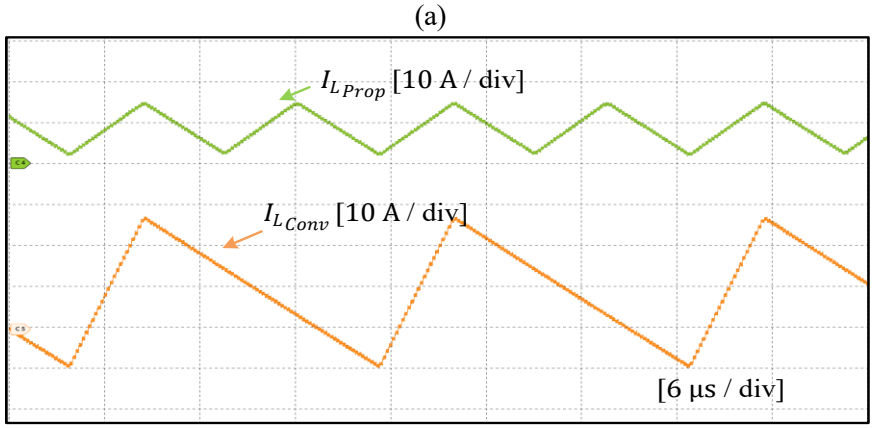

(b)

Fig. 3.11. Experiment results. (a) Inductor current of the proposed ($I_{L_{Prop}}$)and conventional ($I_{L_{Conv}}$) converter. (b) zoom in results of (a).

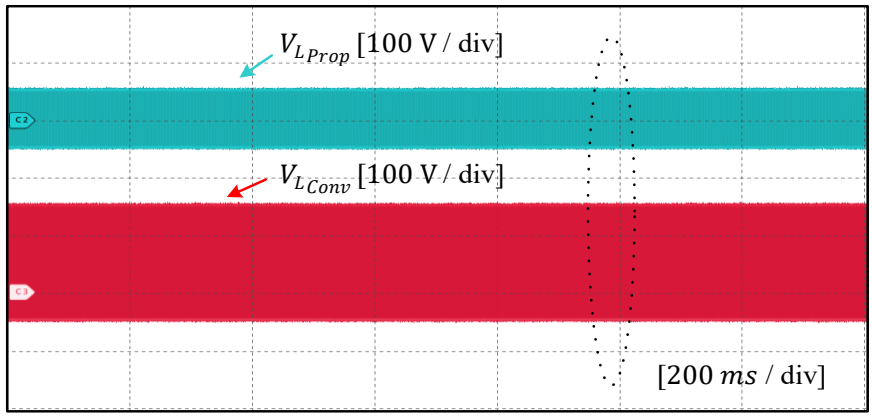

(a)

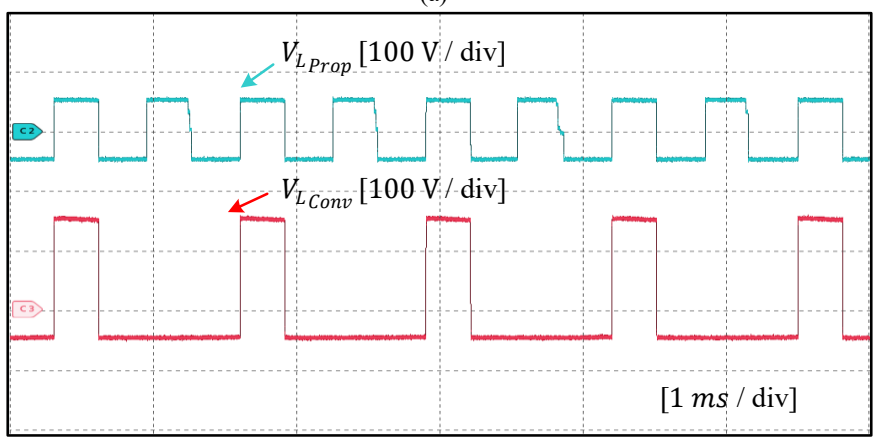

(b)

Fig. 3.12. Experimental results. (a) expanded results of inductor voltage of the proposed and conventional converter ($V_{L_{Conv}}, V_{L_{Conv}}$). (b) Zoom-in results of (a).

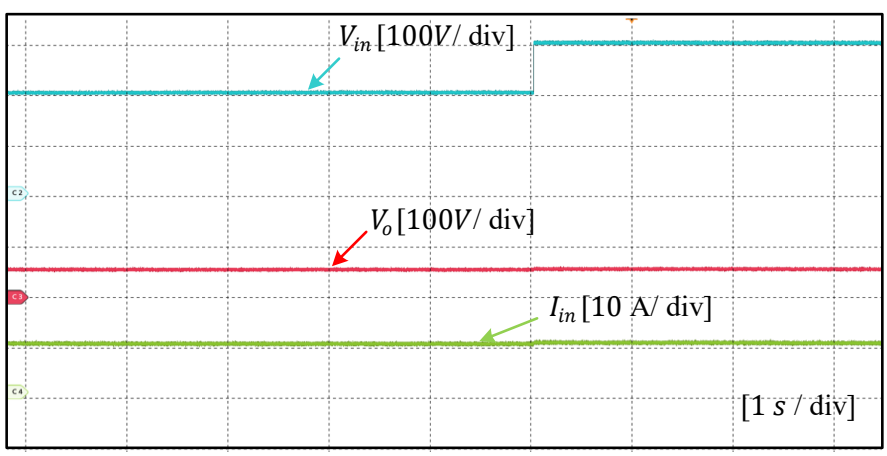

(a)

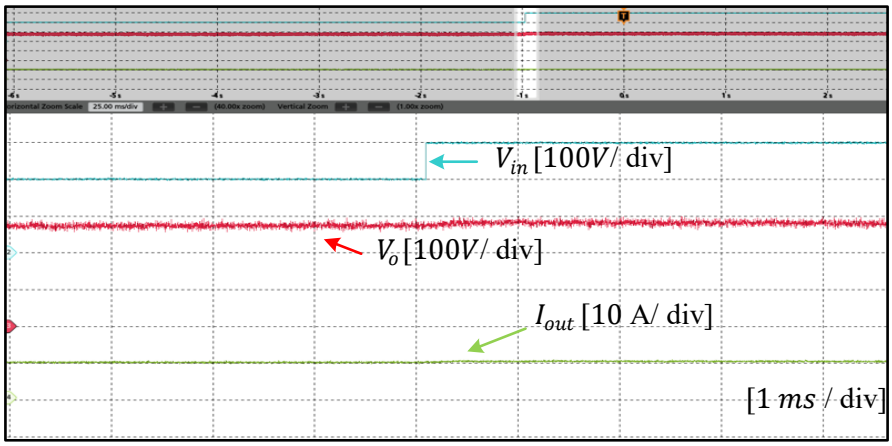

(b)

Fig. 3.13. Experimental results. (a) Expanded results of variation in input voltage vs output voltage and current. (b) Zoom-in results of (a)

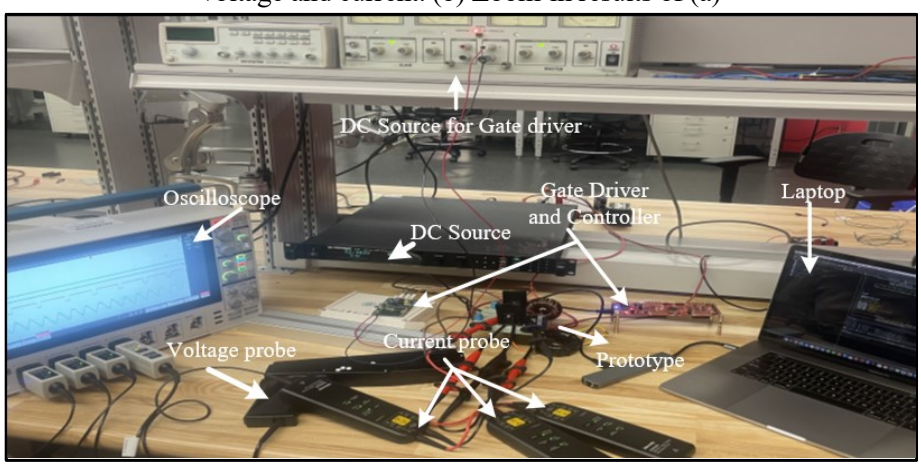

Fig. 3.14. Experimental setup.

3.7. Conclusion

The article introduces a non-isolated Bidirectional DC-DC Converter (BDC) designed for Battery Energy Storage Systems (BESS). It thoroughly discusses the converter's operating principles, specifications, and circuit parameter design. The proposed BDC is highlighted for its ability to handle low output currents, minimize component voltage stresses, and maintain common grounds across input and output ports, making it a suitable interface for battery

storage applications. Additionally, using a small filter inductor reduces output current ripple, effectively safeguarding the BESS and extending its operational lifespan. Experimental results illustrating the performance and ripple comparison further validate the effectiveness of this converter for BESS applications.

References

1. O. Edenhofer, R. Pichs Madruga, Y. Sokona, and IPCC, Eds., *Renewable en ergy sources and climate change mitigation: summary for policymakers and technical summary*. Genf: International Panel of Climate Change, 2011.

2. S.-P. Wang, H. Liao, and J.-F. Chen, "Design and Implementation of a Nov el Bidirectional DC-DC Converter with Coupled Inductor," in *2018 IEEE 7th World Conference on Photovoltaic Energy Conversion (WCPEC) (A Joint Conference of 45t h IEEE PVSC, 28th PVSEC & 34th EU PVSEC)*, Waikoloa Village, HI: IEEE, Jun. 2018, pp. 0644–0649. doi: 10.1109/PVSC.2018.8548196.

3. S. Esmaeili, M. Shekari, M. Rasouli, S. Hasanpour, A. A. Khan, and H. Ha fezi, "High Gain Magnetically Coupled Single Switch Quadratic Modified SEPIC DC -DC Converter," *IEEE Trans. Ind. Appl.*, vol. 59, no. 3, pp. 3593–3604, May 2023, doi: 10.1109/TIA.2023.3250405.

4. B. M. Reddy and P. Samuel, "A comparative analysis of non-isolated bi-dir ectional dc-dc converters," in *2016 IEEE 1st International Conference on Power Elec tronics, Intelligent Control and Energy Systems (ICPEICES)*, Delhi, India: IEEE, Jul. 2016, pp. 1–6. doi: 10.1109/ICPEICES.2016.7853292.

5. F. Mumtaz, N. Zaihar Yahaya, S. Tanzim Meraj, B. Singh, R. Kannan, and O. Ibrahim, "Review on non-isolated DC-DC converters and their control techniques for renewable energy applications," *Ain Shams Eng. J.*, vol. 12, no. 4, pp. 3747–376 3, Dec. 2021, doi: 10.1016/j.asej.2021.03.022.

6. E. Parimalasundar, S. Maneesha, R. Hanish, P. M. Reddy, P. K. Harish, an d P. K. Rao, "Performance Analysis of DC-DC Converter for Electric Vehicle Charg ing Applications," in *2023 7th International Conference on Computing Methodologies and Communication (ICCMC)*, Erode, India: IEEE, Feb. 2023, pp. 1543–1546. doi:

10.1109/ICCMC56507.2023.10084154.

7. A. Chub, D. Vinnikov, R. Kosenko, E. Liivik, and I. Galkin, “Bidirectional DC–DC Converter for Modular Residential Battery Energy Storage Systems,” *IEEE T rans. Ind. Electron.*, vol. 67, no. 3, pp. 1944–1955, Mar. 2020, doi: 10.1109/TIE.201 9.2902828.

8. Z. Wang, P. Wang, B. Li, X. Ma, and P. Wang, “A Bidirectional DC–DC Converter With High Voltage Conversion Ratio and Zero Ripple Current for Battery Energy Storage System,” *IEEE Trans. Power Electron.*, vol. 36, no. 7, pp. 8012–802 7, Jul. 2021, doi: 10.1109/TPEL.2020.3048043.

9. S. B. Santra, D. Chatterjee, and Y. P. Siwakoti, “Coupled Inductor Based S oft Switched High Gain Bidirectional DC-DC Converter With Reduced Input Current Ripple,” *IEEE Trans. Ind. Electron.*, vol. 70, no. 2, pp. 1431–1443, Feb. 2023, doi: 10.1109/TIE.2022.3156153.

10. K. Filsoof and P. W. Lehn, “A Bidirectional Modular Multilevel DC&#x201 3;DC Converter of Triangular Structure,” *IEEE Trans. Power Electron.*, vol. 30, no. 1, pp. 54–64, Jan. 2015, doi: 10.1109/TPEL.2014.2307004.

11. A. Ahmad, R. K. Singh, and R. Mahanty, “Bidirectional quadratic converter for wide voltage conversion ratio,” in *2016 IEEE International Conference on Power Electronics, Drives and Energy Systems (PEDES)*, Trivandrum, India: IEEE, Dec. 2 016, pp. 1–5. doi: 10.1109/PEDES.2016.7914538.

12. A. A. Khan, H. Cha, and J.-S. Lai, “Cascaded Dual-Buck Inverter With Re duced Number of Inductors,” *IEEE Trans. Power Electron.*, vol. 33, no. 4, pp. 2847 –2856, Apr. 2018, doi: 10.1109/TPEL.2017.2701400.

13. M. Forouzesh, Y. P. Siwakoti, S. A. Gorji, F. Blaabjerg, and B. Lehman, “ Step-Up DC–DC Converters: A Comprehensive Review of Voltage-Boosting Techniq

ues, Topologies, and Applications," *IEEE Trans. Power Electron.*, vol. 32, no. 12, p p. 9143–9178, Dec. 2017, doi: 10.1109/TPEL.2017.2652318.

14. S. M. Fardahar and M. Sabahi, "New Expandable Switched-Capacitor/Switch ed-Inductor High-Voltage Conversion Ratio Bidirectional DC–DC Converter," *IEEE T rans. Power Electron.*, vol. 35, no. 3, pp. 2480–2487, Mar. 2020, doi: 10.1109/TPEL .2019.2932325.

15. D. Hulea, N. Muntean, M. Gireada, O. Cornea, and E. Serban, "Bidirectiona l Hybrid Switched-Inductor Switched-Capacitor Converter Topology with High Voltag e Gain," in *2019 21st European Conference on Power Electronics and Applications (EPE '19 ECCE Europe)*, Genova, Italy: IEEE, Sep. 2019, p. P.1-P.10. doi: 10.2391 9/EPE.2019.8915535.

16. A. A. Khan *et al.*, "Coupled-Inductor Buck–Boost Inverter With Reduced C urrent Ripple," *IEEE Trans. Power Electron.*, vol. 35, no. 8, pp. 7933–7946, Aug. 2 020, doi: 10.1109/TPEL.2019.2962668.

17. A. H. Ismail, Z. Ma, A. Al-Hmoud, and Y. Zhao, "A High Frequency Cou pled Inductor Design for High Power Density DC-DC Converters," in *2023 IEEE Ap plied Power Electronics Conference and Exposition (APEC)*, Orlando, FL, USA: IEE E, Mar. 2023, pp. 3275–3280. doi: 10.1109/APEC43580.2023.10131629.

18. G.-R. Zhu, S.-C. Tan, Y. Chen, and C. K. Tse, "Mitigation of Low-Frequen cy Current Ripple in Fuel-Cell Inverter Systems Through Waveform Control," *IEEE Trans. Power Electron.*, vol. 28, no. 2, pp. 779–792, Feb. 2013, doi: 10.1109/TPEL. 2012.2205407.

19. D. B. W. Abeywardana, B. Hredzak, J. E. Fletcher, and G. Konstantinou, " A cascaded boost inverter based battery energy storage system with reduced battery r ipple current," in *IECON 2017 - 43rd Annual Conference of the IEEE Industrial Ele*

ctronics Society, Beijing: IEEE, Oct. 2017, pp. 2733–2738. doi: 10.1109/IECON.2017.8216460.

20. Po-Wa Lee, Yim-Shu Lee, D. K. W. Cheng, and Xiu-Cheng Liu, "Steady-state analysis of an interleaved boost converter with coupled inductors," *IEEE Trans. Ind. Electron.*, vol. 47, no. 4, pp. 787–795, Aug. 2000, doi: 10.1109/41.857959.

21. W. C. Leal, M. O. Godinho, R. F. Bastos, C. R. De Aguiar, G. H. F. Fuzato, and R. Q. Machado, "Cascaded Interleaved DC–DC Converter for a Bidirectional Electric Vehicle Charging Station," *IEEE Trans. Ind. Electron.*, vol. 71, no. 4, pp. 3708–3717, Apr. 2024, doi: 10.1109/TIE.2023.3273281.

22. D. Scire, G. Lullo, and G. Vitale, "Design and Modeling of an Interleaving Boost Converter with Quasi-Saturated Inductors for Electric Vehicles," in *2020 AEIT International Conference of Electrical and Electronic Technologies for Automotive (AEIT AUTOMOTIVE)*, Turin, Italy: IEEE, Nov. 2020, pp. 1–6. doi: 10.23919/AEITAUTOMOTIVE50086.2020.9307424.

23. A. Sferlazza *et al.*, "Robust Disturbance Rejection Control of DC/DC Interleaved Boost Converters with Additional Sliding Mode Component," in *2023 Asia Meeting on Environment and Electrical Engineering (EEE-AM)*, Hanoi, Vietnam: IEEE, Nov. 2023, pp. 01–06. doi: 10.1109/EEE-AM58328.2023.10395325.

24. F. Akbar, H. Cha, H. F. Ahmed, and A. A. Khan, "A Family of Single-Stage High-Gain Dual-Buck Split-Source Inverters," *IEEE J. Emerg. Sel. Top. Power Electron.*, vol. 8, no. 2, pp. 1701–1713, Jun. 2020, doi: 10.1109/JESTPE.2019.2894384.

25. A. A. Khan, H. Cha, and H. F. Ahmed, "An Improved Single-Phase Direct PWM Inverting Buck–Boost AC–AC Converter," *IEEE Trans. Ind. Electron.*, vol. 63, no. 9, pp. 5384–5393, Sep. 2016, doi: 10.1109/TIE.2016.2565461.

26. A. A. Khan, H. Cha, and H. F. Ahmed, "High-Efficiency Single-Phase AC–

AC Converters Without Commutation Problem," *IEEE Trans. Power Electron.*, vol. 31, no. 8, pp. 5655–5665, Aug. 2016, doi: 10.1109/TPEL.2015.2494605.

Chapter IV
A Novel Two-Phase Isolated Buck Converter with Increased Inductor Frequency and Low Diode-bridge stress

Preface

A version of this section of the manuscript chapter has been accepted and submitted in ECCE 2024 Arizona. I, Jamil M Khan the primary author of this paper, and I carried out most of the research work performed the literature reviews, carried out the system design, implementations, and analysis of the results. I also prepared the first draft of the manuscript. The Co-authors, Dr. Ashraf Ali Khan supervised the research, provided the research guide, reviewed, and corrected the manuscript, and contributed research ideas to the actualization of the manuscript.

Reference: "A Novel Two-Phase Isolated Buck Converter with Increased Inductor Frequency and Low Diode-bridge stress "ECCE 2024 Digest ,EC 1092"

Abstract

This paper presents isolated DC-DC Buck converter to address issues in power converters for renewable energy applications. The proposed design features an isolated two-phase buck converter with coupled inductors and a phase-shift interleaving switching scheme. By reducing output current ripples, the system enables high-frequency operation while minimizing filter inductor size and improving the lifetime of energy storage elements (ESE). A significant advancement involves setting the switching frequency for the output inductor at four times the actual switching frequency. Operating the output inductor at four times the switching frequency reduces voltage stress and allows for a more compact inductor size. The proposed converter has no short-circuit issues, thus achieves a very high reliability. Moreover, the reverse recovery issues of the MOSFET body diodes are mitigated. Therefore, the proposed can be operated at a high switching frequency while maintain a high efficiency. Detailed simulations and experimental results are provided.

4.1. Introducntion

The increasing global demand for energy has resulted in extensive fossil fuel consumption, which emits greenhouse gases and exacerbates global warming. This environmental challenge has created an urgent need for sustainable energy solutions, prompting significant growth in renewable energy sources and a transition toward cleaner, more sustainable energy options [1]. With growing concerns about environmental pollution from conventional internal combustion engines (ICGs), electric vehicles (EVs) are gaining increased attention. EVs are not only more environmentally friendly but also more cost-effective to operate compared to their fossil fuel counterparts[2]. The rapid advancement of power electronics converters has further supported the integration of sustainable energy resources for electricity production, facilitating the mass production of EVs[3]. DC-DC converters are utilized in various applications, including DC drives, microgrids [4], automotive industries, and power factor correction devices.[1]

DC-DC converters can be categorized as Unidirectional and Bidirectional converters [5]. Unidirectional converters direct the generated energy to Energy storage elements (ESE) like batteries. Unidirectional converters can be divided into two categories, i.e., Isolated and non-isolated converters. Isolated converters presented in [6] use transformers that provide isolation and high gain for specific applications. However, it comes at the cost of enormous size, switching losses, and stress on switching devices. On the other hand, non-isolated are smaller in size and have no transformers [7], but these are applicable only where galvanic isolation is not required.

In many high-power applications, converters are designed to handle significant current levels. As a result, the inductors become large and bulky, decreasing the converter's power density.[8] However, numerous applications demand compact converters,

making the traditional design less favorable for these uses. Additionally, the switching phenomena induce high current ripples across the converters, which can cause ESE degradation issues and reduce the lifetime of batteries.

To overcome these problems, an interleaving technique is usually preferred [9]. As discussed in [10], the interleaving technique combined with the use of a coupled inductor divides the high current among its interleaving paths, which reduces stress on switching components and increases the power ratings of the converter. Similarly, the doubling frequency effect discussed in [10] at the output inductor make the output filter inductor smaller and reduces the current ripples. This paper proposed a novel isolated buck converter to make the output inductor frequency four times and reduce its voltage stress. As a result the overall size of the output inductor has been decreased significantly. Moreover, the proposed converter has high reliability same as in [11-17]. In addition, the overall efficiency and power density of the converter has been improved. The high power density, low switching stress and current, make it favorable choice for EVs, ESE and Renewable Energy Storage (RES).

The proposed converter topology, switching scheme and operations mode will be discussed in section II. PSIM simulation results are provided in section III. Experimental results are discussed in Section IV and conclusion is added in the last section.

4.2. Proposed Converter and Switching Scheme

The proposed isolated converter is shown in the Fig. 4.1. The converter features four switch legs configuration on input side, each with a MOSFET (S_1, S_2, S_3, S_4) and an external diode (D_1, D_2, D_3, D_4) in series. The first two legs connect to a coupled inductor (CL_a), and the last two connect to a couple inductor (CL_b). Coupled inductors mitigate short-circuit risks, divide current flow among its branches, limit flow through MOSFET body diodes, and double

the switching frequency. The output of the two coupled inductors connects to a transformer (V_{tr}) with an turns ($n_{p=}$ n_s). The transformer provides isolation and step-up/step-down operations. Secondary side components include four diodes (d_1, d_2, d_3, d_4) an output inductor (L_{out}), output filter capacitor (C_o) and load (R_L). The coupled inductor along with the proposed switching strategy enables the output inductor to operate at four times the switching frequency, allowing for a smaller inductor size.

Due to the switching phenomenon, high output current ripples appear in DC-DC converters. To mitigate these issues, interleaving or multi-phasing is often preferred. This design segregates the current to flow through different phases, thereby increasing the power rating of the converter, minimizing the current stress on switches, and reducing the ripple in inductor current. Consequently, the thermal distribution of the converter is significantly improved. These advantages collectively enhance the efficiency and reliability of the converter, ultimately boosting the overall performance of the system. However, the conventional approaches require more switches to reduce the output ripple.

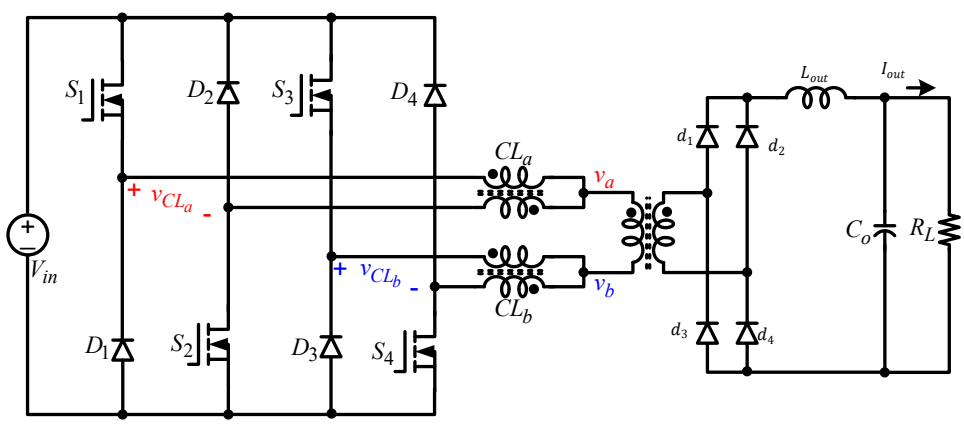

Fig. 4.1. Proposed isolated buck converter.

The proposed converter employs a phase-shifted interleaved PWM switching scheme, depicted in Fig. 4.2. This PWM scheme is generated by comparing four triangular waves, each phase-shifted by 90 degrees, with a reference voltage. This results in a switching scheme that operates in both dead time and overlap time modes as shown in Fig. 3.

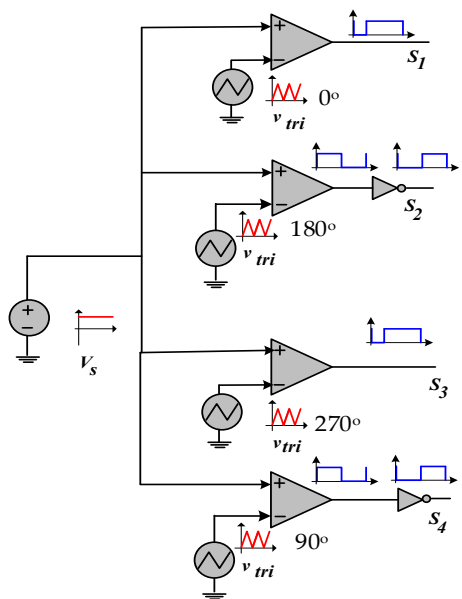

Fig. 4.2. Signals generation of the proposed converter.

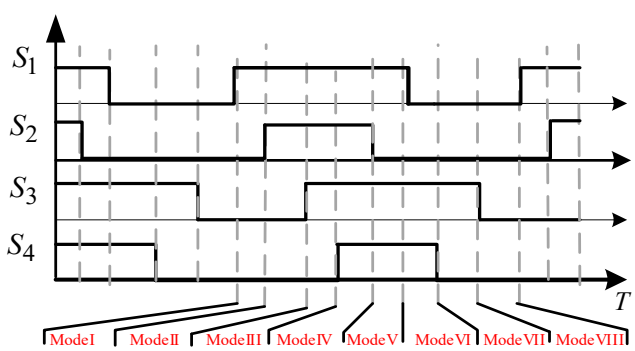

Fig. 4.3. Key Switching waveforms.

4.3. Switching Modes

The proposed converter operates in 8 different modes in a switching cycle as shown in the Fig. 4.3. In this topology, it is assumed that the coupled inductors are identical, and the coupling coefficient, *K* is set to 1, for tight coupling.

The proposed converter has different operation modes for duty ratio ($D>0$) and ($D<0$).

Mode I: In Mode I, illustrated in Fig. 4.4(a), switch S1 is turned ON and all other switches are OFF. On the input side, S1, D3, and D4 conduct, allowing current to flow through these paths. A portion of the current passes through the primary side of the transformer. On the secondary side, diodes d1 and d4 conduct, directing the current through the output inductor.

Mode II: During Mode II, depicted in Fig. 4.4(b), both switches S1 and S2 are ON. On the input side, diodes D3 and D4 conduct, providing a pathway for current. On the secondary side, diodes d2 and d3 conduct, maintaining the flow of current through the output inductor.

Mode III: As shown in Fig. 4.4(c), Mode III involves switches S1, S2, and S3 being ON. On the input side, diode D4 conducts, allowing current to flow. On the secondary side, diodes d2 and d3 continue to conduct the output inductor current, ensuring steady power delivery to the load.

Mode IV: In Mode IV, illustrated in Fig. 4.4(d), all switches S1, S2, S3, and S4 are ON. All diodes on the input side are reverse-biased, preventing current flow through them. On the secondary side, diodes d1 and d4 conduct the output inductor current.

Mode V: Fig. 4.4(e) shows Mode V, where switches S1, S3, and S4 are ON. On the input side, diode D2 conducts, allowing current to flow through this path. On the secondary side, diodes d1 and d4 conduct the output inductor current.

Mode VI :During Mode VI, depicted in Fig. 4.4(f), switches S3 and S4 are ON. On the input side, diodes D1 and D2 conduct, creating parallel current paths. On the secondary side, diodes d2 and d3 conduct the output inductor current, ensuring continuous power delivery to the load.

Mode VII: In Mode VII, shown in Fig. 4.4(g), switch S3 is ON. On the input side, diodes D1, D2, and D4 conduct, providing multiple current paths. On the secondary side, diodes d2 and d3 continue to conduct the output inductor current.

4.4. Simulation Results

The simulation results of the proposed isolated buck converter were obtained from PSIM. Fig. 4.5(a) indicates the simulation results (for turns ratio n=1) of input voltage(V_{in}), output voltage (V_{out}), output current (I_{Lout}) with the corresponding switching signal S1. Fig. 4.5(b) depicts the simulation results indicated in Fig. 5(a) but for turns ratio n=2. Fig. 4.5(c) shows the voltage stress across switches (S_1, S_2, S_3, S_4) and Fig. 4.5(d) shows the voltage stress across diodes (D_1, D_2, D_3, D_4).

Fig. 4.6(a) shows the voltage across the output inductor (V_{Lout}), output inductor current (I_{Lout}) along with the voltage drop across switches (S_1, S_2). Fig. 4.6(b) shows voltage across primary and secondary side of transformer for turn (n=1). Similarly for ratio (n=2) voltages across primary and secondary sides of the transformer are shown in Fig. 4.6(c).

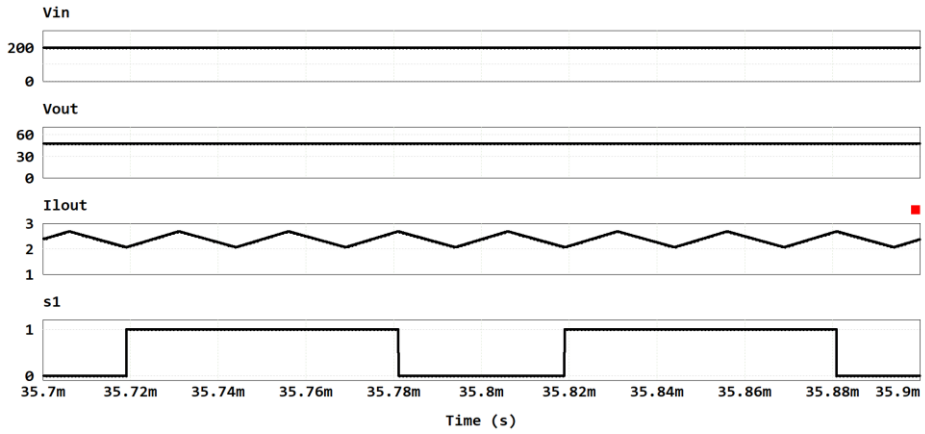
Vin
200
0
Vout
60
30
0
Ilout
3
2
1
s1
1
0
35.7m
35.72m
35.74m
35.76m
35.78m
35.8m
35.82m
35.84m
35.86m
35.88m
35.9m
Time (s)

(a)

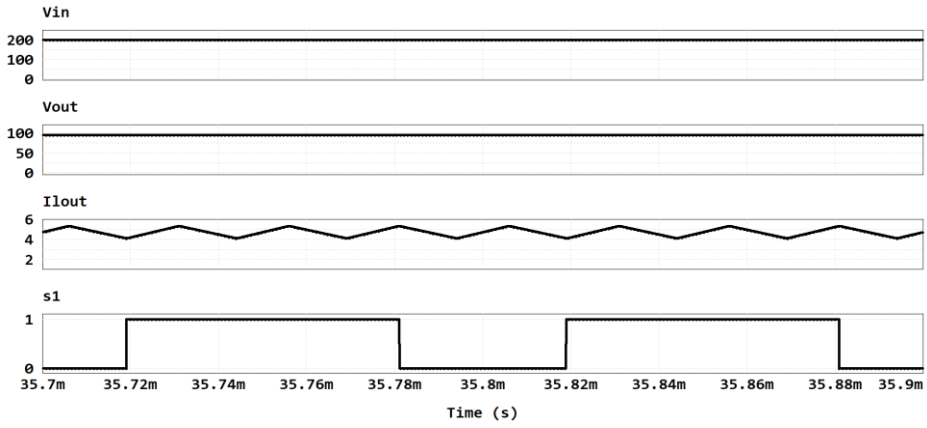
Vin
200
100
0
Vout
100
50
0
Ilout
6
4
2
s1
1
0
35.7m
35.72m
35.74m
35.76m
35.78m
35.8m
35.82m
35.84m
35.86m
35.88m
35.9m
Time (s)

(b)

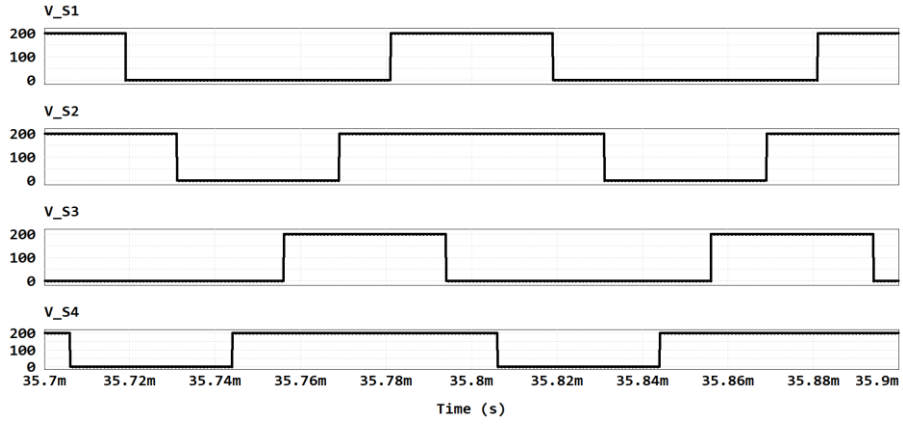
V_S1
200
100
0
V_S2
200
100
0
V_S3
200
100
0
V_S4
200
100
0
35.7m
35.72m
35.74m
35.76m
35.78m
35.8m
35.82m
35.84m
35.86m
35.88m
35.9m
Time (s)

(c)

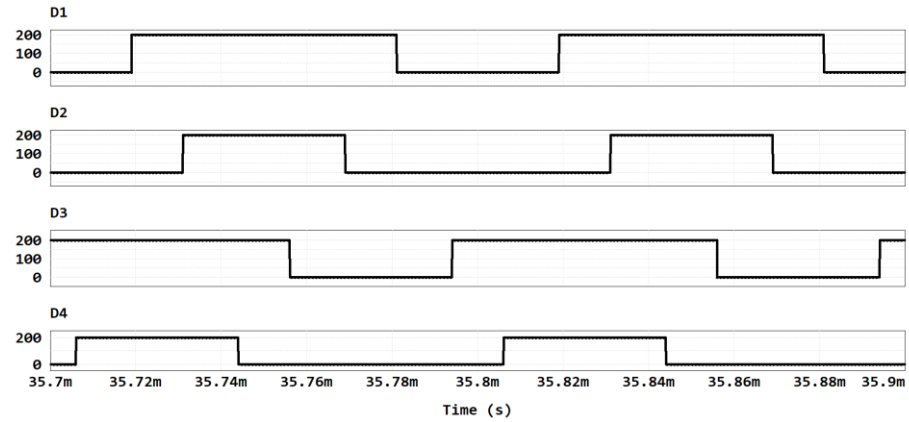

(d)

Fig. 4.5. (a) Simulation waveform for turn ratio, n=1, input voltage, output voltage, output current and switching signal. (b) Simulation results for turn ratio, n=2. (c) Voltage drop across switches (S_1, S_2, S_3, S_4). (d) Voltage across diodes (D_1, D_2, D_3, D_4).

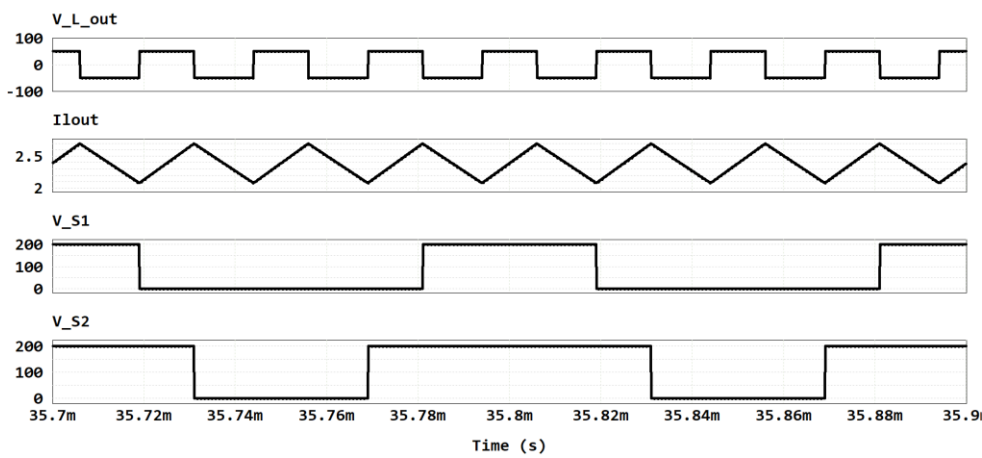

(a)

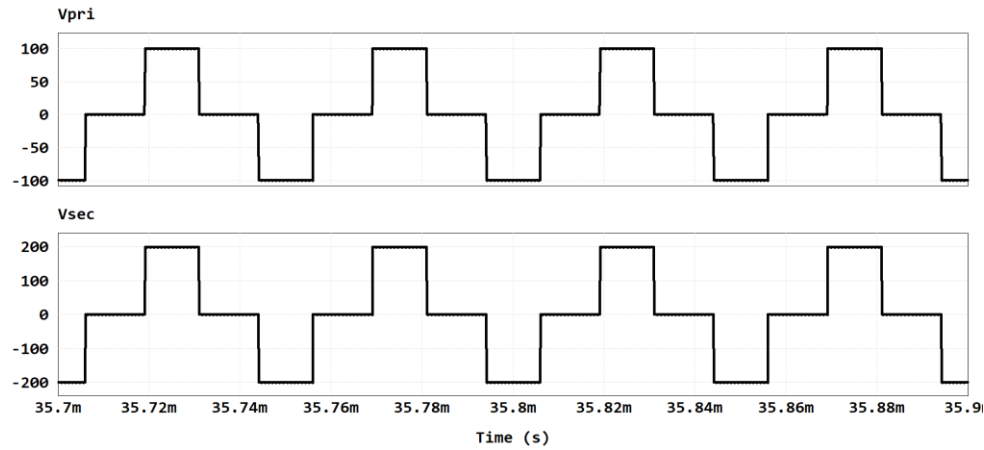

(b)

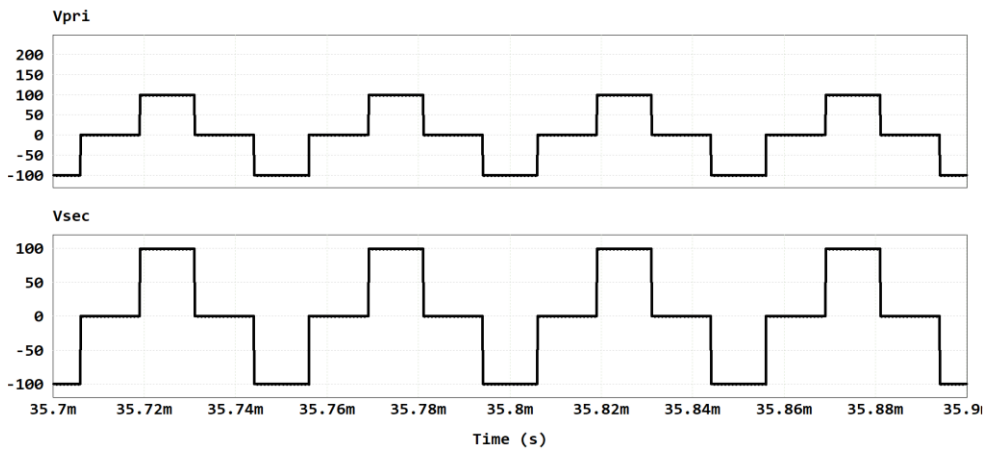

(c)

Fig. 4.6. Simulation results (a) Voltage across inductor, output inductor current, voltage drop across switches (S_1, S_2). (b) Voltage across primary and secondary sides of the isolation transformer for turn ratio, $n=1$. (c) Voltage across primary and secondary sides of the isolation transformer for turn ratio, $n=2$.

4.5. Experimental Results

A 480 W prototype of the proposed converter was built and tested. The specifications and component parameters are given in Table 4.1. The magnetizing inductance of the transformer is 0.5 mH and the turn ratio is 1. The coupling factor (k) for the coupled inductors is set to 1, and the magnetizing inductance of both coupled inductors is 0.5 mH. Fig. 7(a) shows the voltage drop across switches (S_1, S_2,), output current (I_{Lout}) and output voltage (V_{out}). As shown these experimental results validates that the output inductor current frequency is four times the switching frequency. Fig. 7(b) depicts the voltage stresses across switches (S_3, S_4,), and diodes (D_3, D_4). Fig. 7(c) shows voltage stresses across switches (S_1, S_2,), and diodes (D_1, D_2). From Fig. 7(b) and Fig. 7(c), the results clearly show that the stress across the switches is equal to the input voltage. Similarly, the voltage stress across the diodes is reduced to half of the input voltage. Fig. 7(d) indicates the voltage across the primary transformer and output inductor, output inductor current, along with the output voltage.

Table 4. 1. Componenet Specification (Isolated Buck Converter)

Components	*Values*
Input voltage (V_{in})	200 V
Ouptut voltage (V_{out})	48 V
Rated output power	480 W
MOSFET ($S_1 - S_4$)	BYC30JT-600PSQ
Switching frequency (f_s)	50 KHz
Diodes (D_1, D_2)	SDUR3040W
Inductor (L_{out})	0.1 mH
Output Capacitor (C_O)	100 μF

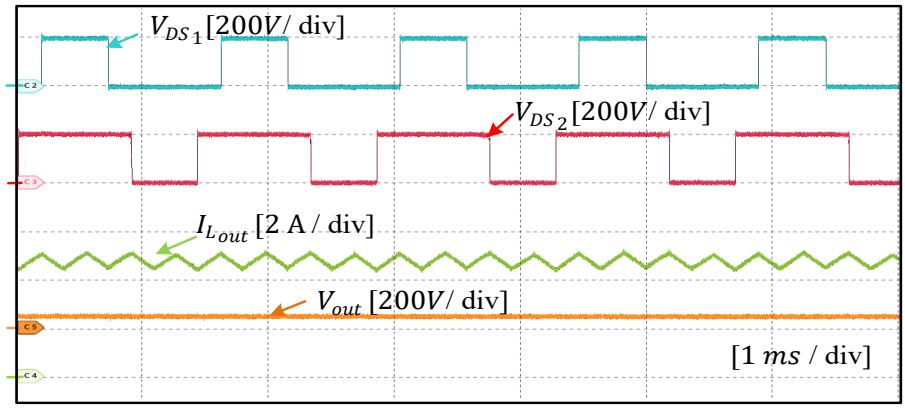
V_{DS_1}[200V/ div]
V_{DS_2}[200V/ div]
$I_{L_{out}}$ [2 A / div]
V_{out} [200V/ div]
[1 ms / div]

(a)

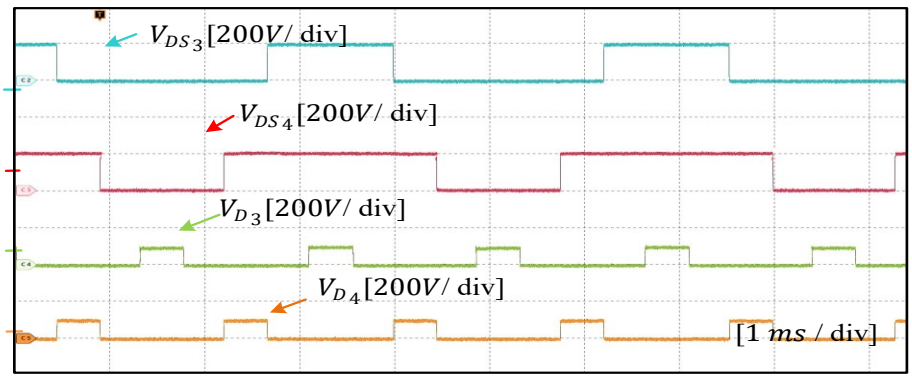
V_{DS_3}[200V/ div]
V_{DS_4}[200V/ div]
V_{D_3}[200V/ div]
V_{D_4}[200V/ div]
[1 ms / div]

(b)

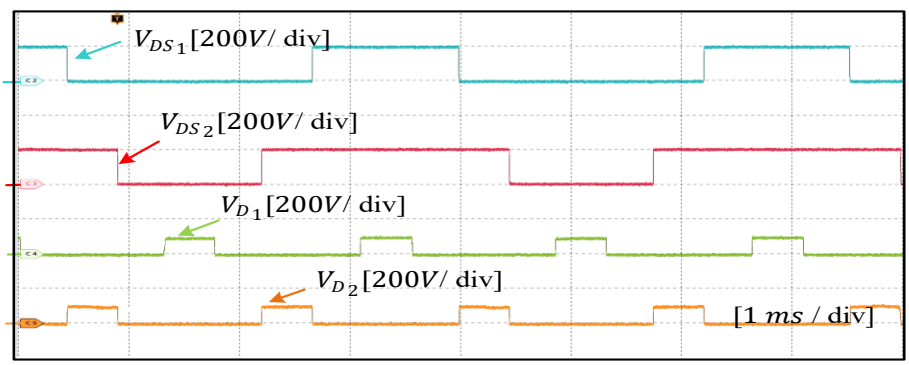
V_{DS_1}[200V/ div]
V_{DS_2}[200V/ div]
V_{D_1}[200V/ div]
V_{D_2}[200V/ div]
[1 ms / div]

(c)

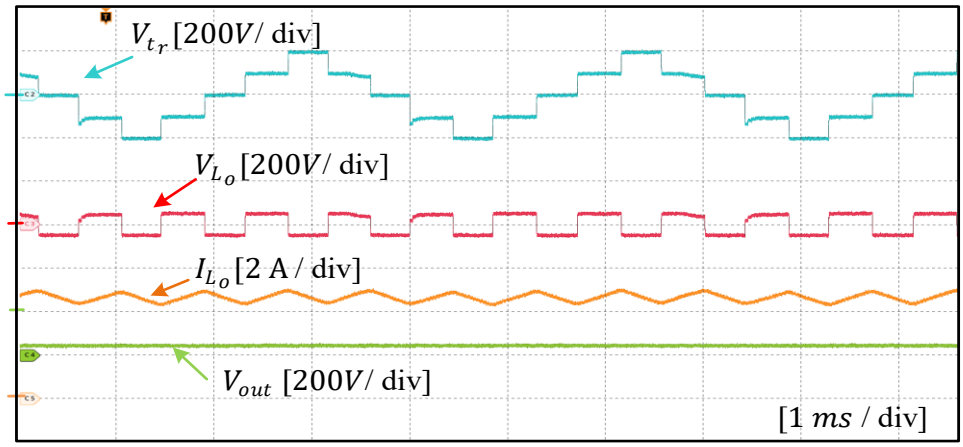

(d)

Fig. 4.7. Experimental results. (a) Voltage drop across switches (S_1, S_2,), output current (I_{Lout}) and voltage (V_{out}). (b) Voltage stress across switches (S_3, S_4,), and diodes (D_3, D_4). (c) Voltage stress across switches (S_1, S_2,), and diodes (D_1, D_2).(d) voltage across the primary of transformer and output inductor (V_{Lout}), output inductor current (I_{Lout}) along with the output voltage (V_{Lout}).

4.6. Conclusion

This article introduces an isolated DC-DC buck converter suitable for battery charging applications in EV and RES. It thoroughly discusses the converter's operating principles, specifications, and circuit parameter design. The proposed buck converter is highlighted for its small magnetic component size, ability to reduce voltage stress on diodes, and specialty in operating the output inductor at four times the switching frequency, enabling the selection of a small filter inductor. A small filter inductor reduces output current ripple, effectively safeguarding the battery and extending its operational lifespan. Experimental results further validate the effectiveness of this converter.

References

[1]. M. Forouzesh, Y. P. Siwakoti, S. A. Gorji, F. Blaabjerg, and B. Lehman, "Step-Up DC-DC Converters: A Comprehensive Review of Voltage-Boosting Techniques, Topologies, and Applications," *IEEE Trans. Power Electron.*, vol. 32, no. 12, pp. 9143–9178, Dec. 2017, doi: 10.1109/TPEL.2017.2652318.

[2]. H. Zhu, D. Zhang, X. Liu, M. Zhang, and B. Zhang, "A Family of Interleaved Boost Converters for Battery Discharging in Space Applications," *IEEE Trans. Power Electron.*, vol. 38, no. 2, pp. 1887–1900, Feb. 2023, doi: 10.1109/TPEL.2022.3211837.

[3]. Y. Du, X. Zhou, S. Bai, S. Lukic, and A. Huang, "Review of non-isolated bi-directional DC-DC converters for plug-in hybrid electric vehicle charge station application at municipal parking decks," in *2010 Twenty-Fifth Annual IEEE Applied Power Electronics Conference and Exposition (APEC)*, Palm Springs, CA, USA: IEEE, Feb. 2010, pp. 1145–1151. doi: 10.1109/APEC.2010.5433359.

[4]. K. R. Kothapalli, M. R. Ramteke, H. M. Suryawanshi, N. K. Reddi, and R. B. Kalahasthi, "A Coupled Inductor Based High Step-Up Converter for DC Microgrid Applications," *IEEE Trans. Ind. Electron.*, vol. 68, no. 6, pp. 4927–4940, Jun. 2021, doi: 10.1109/TIE.2020.2992019.

[5]. K. M. Tan, V. K. Ramachandaramurthy, and J. Y. Yong, "Integration of electric vehicles in smart grid: A review on vehicle to grid technologies and optimization techniques," *Renew. Sustain. Energy Rev.*, vol. 53, pp. 720–732, Jan. 2016, doi: 10.1016/j.rser.2015.09.012.

[6]. S.-P. Wang, H. Liao, and J.-F. Chen, "Design and Implementation of a Novel B

idirectional DC-DC Converter with Coupled Inductor," in *2018 IEEE 7th World Conference on Photovoltaic Energy Conversion (WCPEC) (A Joint Conference of 45th IEEE PVSC, 28th PVSEC & 34th EU PVSEC)*, Waikoloa Village, HI: IEE E, Jun. 2018, pp. 0644–0649. doi: 10.1109/PVSC.2018.8548196.

[7]. F. Mumtaz, N. Zaihar Yahaya, S. Tanzim Meraj, B. Singh, R. Kannan, and O. I brahim, "Review on non-isolated DC-DC converters and their control techniques for renewable energy applications," *Ain Shams Eng. J.*, vol. 12, no. 4, pp. 3747–3763, Dec. 2021, doi: 10.1016/j.asej.2021.03.022.

[8]. M. Marracci, P. Bolognesi, A. Buffi, G. Caposciutti, and B. Tellini, "Analysis of Current Ripple effect on Lithium batteries," in *2020 IEEE 20th Mediterranean Electrotechnical Conference (MELECON)*, Palermo, Italy: IEEE, Jun. 2020, pp. 109–113. doi: 10.1109/MELECON48756.2020.9140598.

[9]. A. A. Khan *et al.*, "Coupled-Inductor Buck–Boost Inverter With Reduced Current Ripple," *IEEE Trans. Power Electron.*, vol. 35, no. 8, pp. 7933–7946, Aug. 202 0, doi: 10.1109/TPEL.2019.2962668.

[10]. J. M. Khan, A. A. Khan, and M. Jamil, "A Novel Non-Isolated Bidirectiona l DC-DC Converter with Improved Current Ripples for Low-Voltage On-Board C harging," *Energies*, vol. 17, no. 14, p. 3570, Jul. 2024.

[11]. U. A. Khan and J. -W. Park, "Phase-Shifted Cascaded Dual-Buck AC–AC Converter With Less Number of Inductors," in *IEEE Transactions on Power Elec tronics*, vol. 39, no. 6, pp. 7264-7277, June 2024.

[12]. U. A. Khan, J. Lee and J. -W. Park, "An Improved Cascaded Dual-Buck A C-AC Converter," *2020 IEEE 9th International Power Electronics and Motion Co ntrol Conference (IPEMC2020-ECCE Asia)*, Nanjing, China, 2020, pp. 1248-1253.

[13]. A. A. Khan and H. Cha, "Dual-Buck-Structured High-Reliability and High-E

fficiency Single-Stage Buck–Boost Inverters," in *IEEE Transactions on Industrial Electronics*, vol. 65, no. 4, pp. 3176-3187, April 2018.

[14]. A. A. Khan, H. Cha and H. F. Ahmed, "High-Efficiency Single-Phase AC–AC Converters Without Commutation Problem," in *IEEE Transactions on Power Electronics*, vol. 31, no. 8, pp. 5655-5665, Aug. 2016.

[15]. W. Li and X. He, "A Family of Isolated Interleaved Boost and Buck Conv erters With Winding-Cross-Coupled Inductors," in *IEEE Transactions on Power El ectronics*, vol. 23, no. 6, pp. 3164-3173, Nov. 2008.

[16]. H. Mao, L. Yao, J. Liu and I. Batarseh, "Comparison study of inductors cu rrent sharing in non-isolated and isolated DC-DC converters with interleaved stru ctures," *31st Annual Conference of IEEE Industrial Electronics Society, 2005. IEC ON 2005.*, Raleigh, NC, USA, 2005, pp. 7.

[17]. O. Kirshenboim and M. M. Peretz, "High-Efficiency Nonisolated Converter With Very High Step-Down Conversion Ratio," in *IEEE Transactions on Power Electronics*, vol. 32, no. 5, pp. 3683-3690, May 2017.

Chapter V
Conclusions and Future Work

5.1. Conclusion

This thesis has presented the design, analysis, and implementation of advanced bidirectional and unidirectional DC-DC converters for applications in renewable energy storage and electric vehicle battery charging systems. The family of bidirectional converters, featuring a coupled inductor and switch cell structure, has been shown to effectively reduce current ripple and inductor size while enabling high-frequency operation. These converters also address challenges related to reverse recovery losses and common mode currents, offering reliable and efficient solutions for bidirectional power flow. The findings highlight the potential for these designs to enhance energy efficiency in various energy storage applications.

Furthermore, the development of a two-phase isolated buck converter has demonstrated significant improvements in compactness and ripples reduction. This design employ coupled inductors and interleaving switching schemes, which minimize output current ripples and component sizes while reducing voltage stress and reverse recovery losses. Through simulations and experimental validation, these converters have shown suitability for high-performance applications in on-board charging and renewable energy systems. Overall, the work presented in this thesis contributes to the advancement of power electronic converters that meet the growing demands of modern energy storage systems.

5.2. Key Findings

The design, analysis, and implementation of advanced power electronics DC-DC converters i.e, Family of bidirectional DC-DC converters with a focus on boost convert will low ripples and compact size, a bidirectional buck converter for low voltage on-board charging,

and a unidirectional isolated buck converter with low voltage stree and four times output inductor current frequenc are presented in this thesis. These converters have addressed the the key challenges in bidirectional and unidirectional power flow in renewable energy storage and battery charging systems in EVs.

5.2.1. Family of Bidirectional DC-DC Converter using coupled inductor

One key finding of this thesis is the development of bidirecitional DC-DC converters family using coupled inductor and switch cell structure. The proposed design significantly reduces current ripple and inductor size by effectively doubling the switching frequency of the filter inductors. This allows for high-frequency operation with MOSFETs and fast diodes, avoiding reverse recovery issues. The converter is also highly reliable, with no short-circuit concerns and no need for dead time, leading to improved voltage gain and reduced waveform distortion. Additionally, the converter maintains a common ground between input and output terminals, mitigating common mode current issues. While this study focuses on a boost-type converter, the findings are applicable to other configurations in the family.

5.2.2. A Novel non-isolated Bidirectional DC-DC Buck Converter

Another key finding of this thesis is the development of a novel bidirectional DC-DC buck converter optimized for on-board charging applications. The converter features a coupled inductor and an interleaving switching scheme to reduce output current ripples and minimize the size of the filter inductor. By optimizing the switching frequency of the output inductor to be twice the actual switching frequency, the converter significantly reduces component size. The use of MOSFETs with fast recovery diodes helps mitigate reverse recovery losses and reducing stress on components. The experimental results show that the proposed converter achieves very low current ripples compared to conventional designs. Additionally, the

converter preserves a common ground between input and output terminals, eliminating common mode current issues. The design was validated through the development and testing of a 460-W buck converter prototype, demonstrating improvements in efficiency, reliability, and compactness for bidirectional DC-DC conversion systems.

5.2.3. Novel Two-phase Isolated Buck converter

The two phase isolated DC-DC Buck converter addresses issues in power converters for renewable energy applications. The proposed design features an isolated two-phase buck converter with coupled inductors and a phase-shift interleaving switching scheme. By reducing output current ripples, the system enables high-frequency operation while minimizing filter inductor size and improving the lifetime of energy storage elements (ESE). A significant advancement involves setting the switching frequency for the output inductor at four times the actual switching frequency. Operating the output inductor at four times the switching frequency reduces voltage stress and allows for a more compact inductor size. The proposed converter has no short-circuit issues. Moreover, the reverse recovery issues of the MOSFET body diodes are mitigated. Therefore, the proposed can be operated at a high switching frequency. Detailed simulations and experimental results are provided.

5.3. Future Work

5.2.1. Exploring high power ratings

- Integrating the developed converters into Vehicle-to-Grid (V2G) and Grid-to-Vehicle (G2V) systems to enable bidirectional energy transfer between electric vehicles (EVs) and the grid.

- Enhancing converter designs for seamless and efficient bidirectional power flow, ensuring minimal energy losses during both charging (G2V) and discharging (V2G) operations.

5.2.2. Vehicle to Grid (V2G) and Grid to Vehicle (G2V) Applications

- Integrating the developed converters into Vehicle-to-Grid (V2G) and Grid-to-Vehicle (G2V) systems to enable bidirectional energy transfer between electric vehicles (EVs) and the grid.
- Addressing the unique challenges of grid stability and renewable energy integration by enabling EVs to act as energy storage units that can supply power back to the grid during peak demand.
- Optimizing the converter's reliability and efficiency to support the growing role of EVs in smart grid applications and distributed energy management systems.

5.2.3. Making the converter further smaller

To achieve this goal, our future plan is to integrating the coupled inductor and filter inductor onto a single magnetic core that will reduce the overall size and complexity of the converter.we will also consider leveraging leakage inductance from the coupled inductor to serve as the filter inductor, eliminating the need for an additional inductor.

List of Publications

Articles in Journal

- Khan, J.M.; Khan, A.A.; Jamil, M. A Novel Non-Isolated Bidirectional DC-DC Converter with Improved Current Ripples for Low-Voltage On-Board Charging. Energies 2024, 17, 3570. https://doi.org/10.3390/en17143570

Article in IEEE Conference

- Khan,Jamil and A. A. Khan. (2024). "A Novel Two-Phase Isolated Buck Converter with Increased Inductor Frequency and Low Diode-bridge stress "ECCE 2024 Digest ,EC 1092. The paper is accepted in ECCE 2024 Arizona , US.

- Khan,Jamil and A.A. Khan (2023), "A novel bidirectional Buck converter using switching cell stracture". NECEC 2023. This paper is accepted and presented at NECEC 2023 Conference. The manuscript is submitted to the MUN Repository.